

Thiophene conversion under mild conditions over a ZSM-5 catalyst

Lisette Jaimes^a, M. Lujan Ferreira^b, Hugo de Lasa^{a,*}

^aChemical Reactor Engineering Centre, Department of Chemical and Biochemical Engineering, Faculty of Engineering, University of Western Ontario, London, Ontario, Canada N6A 5B9

^bPLAPIQUI, Universidad Nacional del Sur, La Carrindanga Km 7, 8000 Bahía Blanca, Argentina

ARTICLE INFO

Article history:

Received 10 October 2008

Received in revised form 26 January 2009

Accepted 27 January 2009

Available online 24 February 2009

Keywords:

Thiophene

Catalyst selectivity

Zeolites

ZSM-5

Thermodynamics

Reaction mechanisms

ABSTRACT

Refiners are nowadays actively considering the post-treating FCC gasoline processes as a viable and less costly approach for meeting sulfur environmental regulations. Most promising catalytic desulfurization processes do not require hydrogen addition, including between others the use of zeolites as adsorbents/catalysts. This type of desulfurization leads to the formation of significant amounts of coke, requiring keeping high catalyst activity a continuous twin fluidized bed system (fluidized-bed reactor, fluidized bed regenerator). This study evaluates the catalytic conversion of thiophene and/or thiophene in *n*-octane mixtures. Catalytic experiments are carried out in the CREC riser simulator under mild conditions, using H-ZSM5 zeolite dispersed in a silica matrix. The experimental results obtained demonstrate a higher selective conversion of thiophene over *n*-octane. It is shown that thiophene conversion proceeds via ring opening and alkylation yielding H₂S, alkyl-thiophenes, benzothiophene, and coke, with no measurable thiophene saturation or dimerization reactions observed. The experimental results are also supported with an extensive thermodynamic analysis that includes all the possible thiophene conversion pathways over zeolites. On this basis and using as a reference the observable measurable species, a reaction network is proposed to represent the thiophene catalytic conversion under the suggested gasoline post treatment conditions.

© 2009 Elsevier Ltd. All rights reserved.

1. Introduction

Regulations aiming at a drastic reduction of sulfur emissions by imposing a very low concentration of this element in fuels, with limits of 30 ppm in gasoline and 15 ppm in diesel, are in effect since 2004 (Babich and Moulijn, 2003). FCC gasoline is by far the most important sulfur emission contributor, up to 85–95%. To address this problem one possible approach is FCC gasoline hydrotreating. However, hydrogenating decreases gasoline quality reducing octane number. The use of hydrogen also adds important costs. This explains why the latest gasoline desulfurization studies are orientated to desulfurization processes not requiring the use of hydrogen (Jaimes et al., 2008). In this respect, some of the most promising catalytic desulfurization processes that do not need hydrogen addition include the use of zeolites as adsorbents/catalysts.

Thiophenic species represents a large fraction of the total sulfur content in FCC gasoline (60 wt% and over) (Yin and Xia, 2004). Selective adsorption and reaction of thiophene in model hydrocarbons mixtures using zeolites, has been widely investigated (Jaimes et al., 2008). This type of desulfurization leads to significant levels of coke, as a result and in order to maintain catalyst activity, it has been

proposed to be implemented in a fluidized bed reactor and fluidized bed regenerator system.

On this basis, the present research evaluates the conversion of thiophene on H-ZSM5 zeolite crystallites dispersed in a silica matrix following gasoline production in FCC units (post treatment process). Experiments are carried out in the CREC fluidized riser simulator (de Lasa, 1992) under mild conditions using thiophene in *n*-octane mixtures, as representatives of gasoline. The experimental results together with thermodynamic evaluations of the possible thiophene conversion pathways allow identifying the most probable thiophene over zeolite H-ZSM5 reaction network.

2. Thermodynamic analysis of thiophene conversion over zeolites

Different reaction pathways of thiophene conversion over zeolites (USY, H-ZSM5, HY, MCM-22) have been suggested (Jaimes et al., 2008). These mechanisms can be summarized as follow:

- (a) *Adsorption of thiophene and ring opening*: This pathway involves thiophene hydrogen bonding to the SiOHAl groups of the zeolite. This is followed by ring opening involving an adsorbed intermediate, tentatively described as olefin-thiol-like species (Garcia and Lercher, 1992, 1993; Shan et al., 2002). In the absence of a hydrogen donor, this adsorbed intermediate desorbs

* Corresponding author. Tel.: +1 519 661 2144; fax: +1 519 850 2931.
E-mail address: hdelasa@eng.uwo.ca (H. de Lasa).

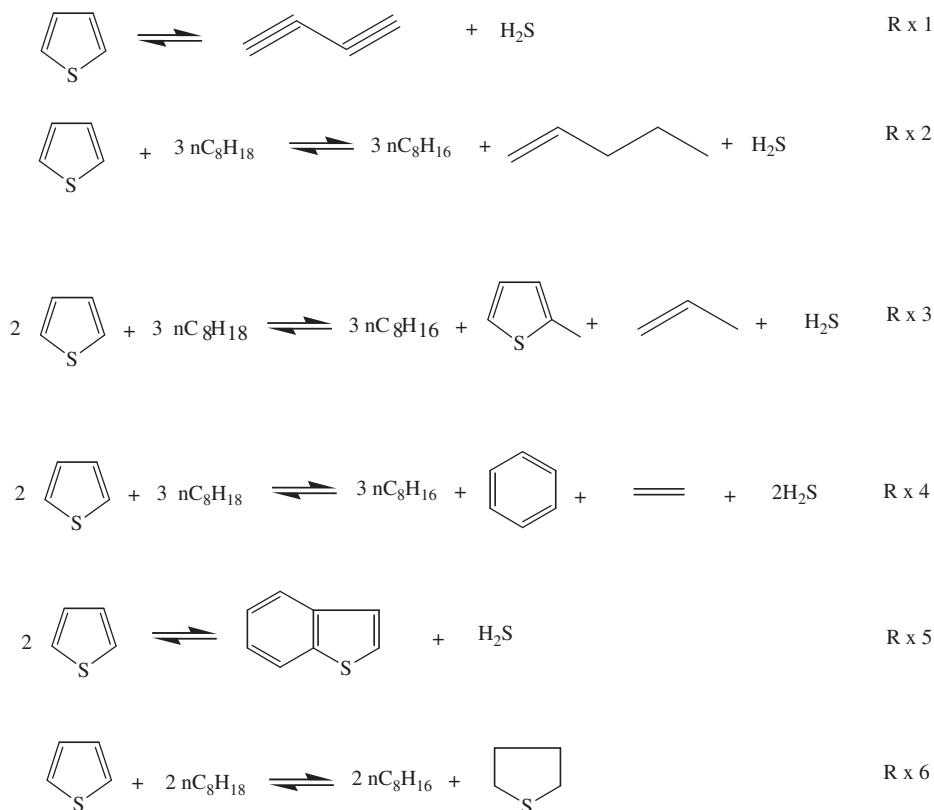


Fig. 1. Set of thiophene over zeolites reactions evaluated thermodynamically (reactions from 1 to 6).

as butadiene plus H₂S through β -elimination (refer to reaction 1, Fig. 1) (Welters et al., 1994; Saintigny et al., 1999). With pre-hydrogenation, however, there is desorption of butadiene and H₂S (Saintigny et al., 1999; Shan et al., 2002). Moreover, via hydrogen transfer, the dibutene species can be converted to butene and even butane (refer to reaction 2, Fig. 1) (Shan et al., 2002).

- (b) *Adsorption of thiophene, ring opening and polymerization with another thiophene molecule:* This step entails an adsorbed mercaptan with two double bonds. Ring opening of this thiophene leads to polymerization with another thiophene molecule. After carbonium ion isomerization and hydrogen transfer, the C–S bond at position β breaks, and H₂S and butenyl-thiophene are formed. In the presence of a hydrogen donor, the butenyl-thiophene is converted, after hydrogen transfer, producing methyl-thiophene and propylene (refer to reaction 3, Fig. 1) (Shan et al., 2002; Chica et al., 2004) or benzene and ethylene (see reaction 4, Fig. 1) (Chica et al., 2004). On the other hand, cyclization of adsorbed butenyl-thiophene produces benzothiophene (reaction 5, Fig. 1) (Shan et al., 2002; Chica et al., 2004). Benzothiophene can also be formed via Diels–Alder condensation, thiophene molecules reacting with adsorbed thiophene derived species (Jaimes et al., 2008).
- (c) *Thiophene hydrogenation and cracking:* This step represents a possible path to explain the transformation of thiophene into butadiene via tetra-hydro-thiophene. This mechanism suggests that first thiophene reacts with hydrogen forming tetra-hydro-thiophene (refer to reaction 6, Fig. 1), and then tetra-hydro-thiophene decomposes to produce H₂S and butadiene (Fu et al., 2000; Wang et al., 2000).
- (d) *Alkylation of thiophene, dealkylation and/or cyclization of alkyl-thiophene:* Alkylation of thiophene can occur via competitive adsorption of thiophene and an olefin adsorbed on the zeolite

acid sites. This step may be followed by the bimolecular reaction of adsorbed species (Belliere et al., 2004), or by the initial formation of the carbenium ion by protonation of thiophene on a Brønsted acid site, followed by a reaction with an olefin (Valla et al., 2006) (refer to reactions 7, 11, 12 and 13, Fig. 2). Furthermore, the production of short alkyl-thiophenes (C₁ and C₂ thiophenes) can initially involve the alkylation of thiophene to produce a long chain alkylated thiophene, followed by proton attack on a sigma C–C bond in the alkyl chain, yielding an olefin and a short alkyl-thiophene (see reactions 8 and 9, Fig. 2) or a paraffin and an alkenyl-thiophene. Finally, the cyclization of a long chain alkylated thiophene can produce benzothiophene (reaction 10, Fig. 2) or alkyl-benzothiophenes (Valla et al., 2006).

- (e) *Dimerization of thiophene:* This reaction step involves adsorption of thiophene in alkoxide species without ring opening (Jaimes et al., 2008). This may be followed by reaction with another thiophene molecule (refer to reaction 14, Fig. 2) (Richardreau et al., 2004; Delitala et al., 2008). Condensation of more than two thiophene molecules followed by hydrogen transfer reactions may also contribute.

In order to review all the possible reaction steps of thiophene, a thermodynamic analysis is carried out in the present study. This analysis takes as the basis a set of reactions, carefully selected adequate to represent the different pathways of thiophene conversion over zeolites described above (Figs. 1 and 2). Regarding the reactions that involve hydrogen transfer from an external source, *n*-octane is selected as the representative model specie. Moreover, ethylene, propylene, and 1-butene are used as the available olefin species for alkylation. It is expected that the proposed approach allows the identification of most thermodynamically favored reaction steps.

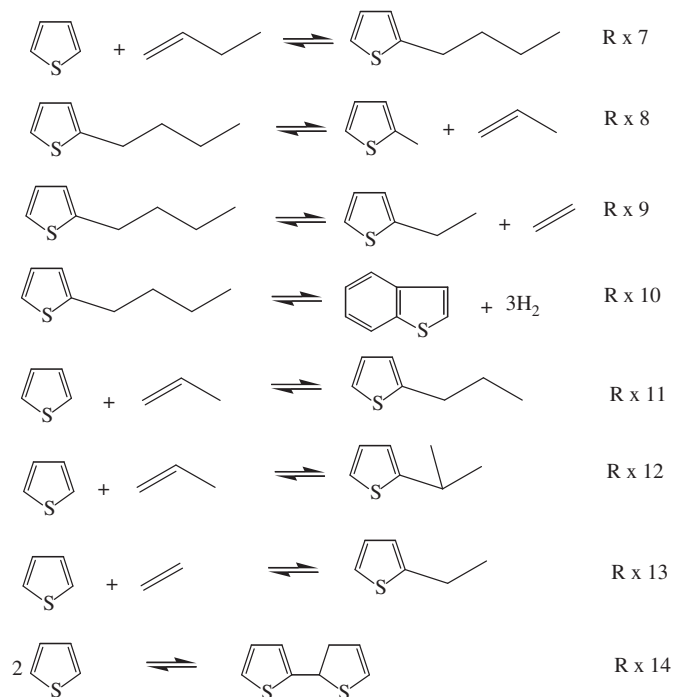


Fig. 2. Set of thiophene over zeolites reactions evaluated thermodynamically (reactions from 7 to 14).

To develop the thermodynamic analysis of the present study, various thermodynamic parameters including enthalpy of reaction, equilibrium constants, and equilibrium conversions were evaluated. However, and because no experimental property data of most of the thiophene related species of the present study is available, the majority of the thermodynamic parameters were as a result, calculated. Also and for the sake of simplicity, the 2-alkyl-thiophenes were used to represent the alkyl-thiophene isomer species lump.

Several methods can be considered to estimate the enthalpy of formation (ΔH_f^0) of organic compounds using the ideal-gas approximation (Stull et al., 1969; Poling et al., 2001). The Joback and Reid's (1987) assigns a specific contribution to each molecular group (for instance $-\text{CH}_3$, $-\text{NH}_2$, etc.) forming a molecule, with these group contributions being added to define a thermodynamic property.

Thus, Joback and Reid's method used in the present study, estimates both ΔH_f^0 , and the polynomial coefficients that relate C_p^0 with temperature as follow:

$$\Delta H_{f,298}^0 = 68.29 + \sum \quad (1)$$

$$C_p^0 = \sum(a) - 37.93 + \left[\sum(b) + 0.210 \right] T + \left[\sum(c) - 3.91 \times 10^{-4} \right] T^2 + \left[\sum(d) + 2.06 \times 10^{-7} \right] T^3 \quad (2)$$

with the \sum representing the addition of the product between frequency of a particular group appears in a molecule compound and the group contribution value.

Values of group contributions were obtained from Joback and Reid (1987). When experimental thermodynamic properties were available for comparisons, it was observed that deviations between calculated and experimental C_p^0 and ΔH_f^0 at 298 K values were lower than 6%.

Regarding the enthalpy of reaction at various temperatures (Figs. 3–5) it was then calculated using the following equation:

$$\Delta H_{rxn,T}^0 = \Delta H_{rxn,298}^0 + \int_{298}^T \left[\sum v_i C_{p,i} \right] dT \quad (3)$$

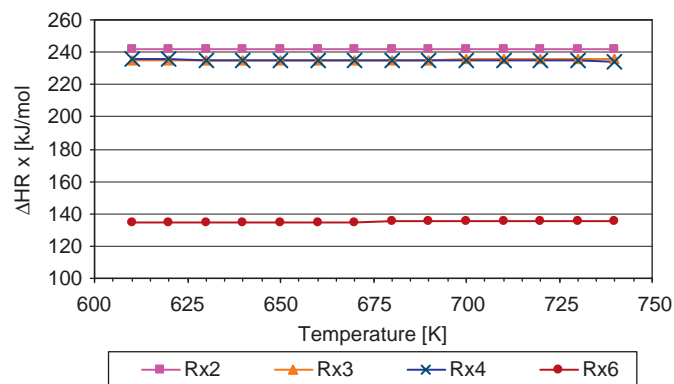


Fig. 3. Reaction enthalpies (ΔH_{rxn}^0) at different temperatures for thiophene ring opening and/or hydrogen transfer reactions (reactions 2, 3, 4 and 6).

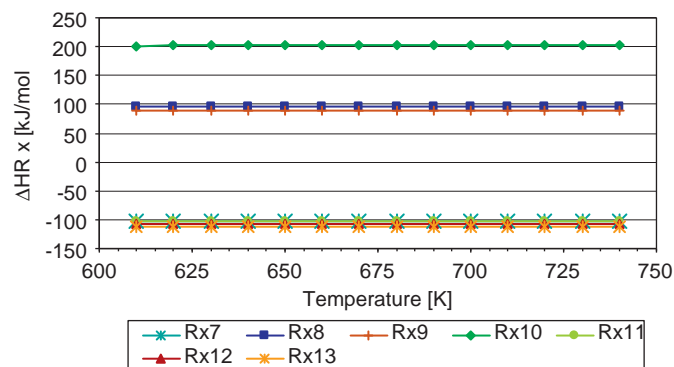


Fig. 4. Reaction enthalpies (ΔH_{rxn}^0) at various temperatures for thiophene alkylation reactions (from reactions 7 to 13).

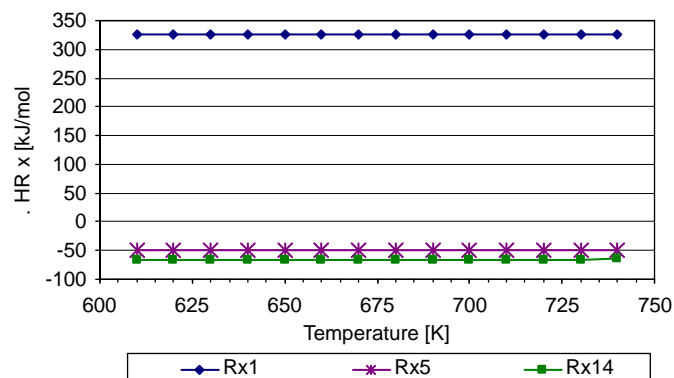


Fig. 5. Reaction enthalpies (ΔH_{rxn}^0) at various temperatures for reactions without a hydrogen donor or co-reactant (reactions 1, 5, and 14).

with $\Delta H_{rxn,298}^0$ being the difference between the enthalpy of formation of products and reactants at 298 K, for the reaction under consideration, and v_i the stoichiometric coefficients.

As shown in Figs. 4 and 5, thiophene alkylation (reactions 7, 11, 12, and 13), thiophene dimerization (reaction 14) and cyclization (reaction 5) are exothermic reactions in 620–720 K range. Therefore, they are thermodynamically favored at lower temperatures. On the other hand, reactions that involve thiophene ring opening (reactions from 1 to 4), hydrogen addition (reaction 6) or cracking (reactions from 8 to 10) are endothermic and as a result, they are thermodynamically favored at higher temperatures.

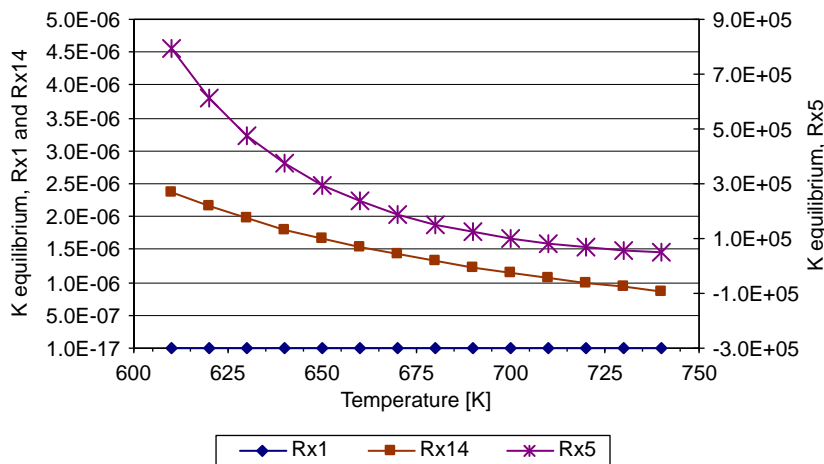


Fig. 6. Influence of temperature on the thermodynamic equilibrium constants for reactions without a hydrogen donor or co-reactant (reactions 1, 5, and 14).

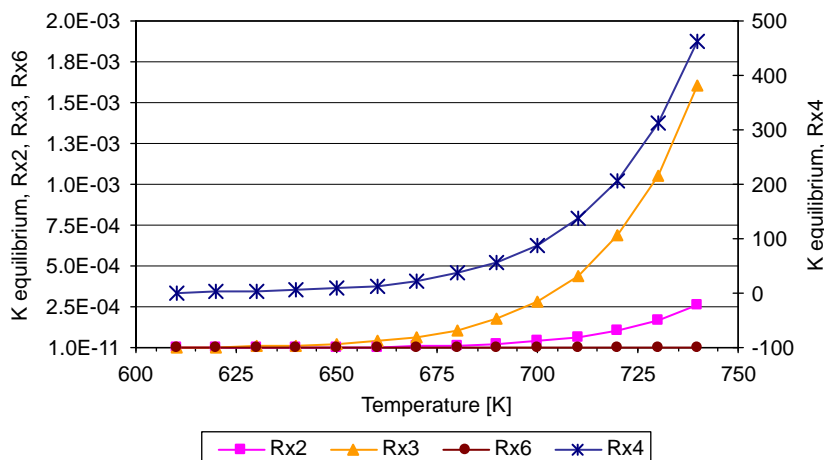


Fig. 7. Influence of temperature on the thermodynamic equilibrium constants for reactions involving thiophene ring opening and hydrogen transfer (reactions 2, 3, 4, and 6).

Regarding the reaction equilibrium constants they were calculated using Eq. (4), with the Gibbs energy of reaction obtained as the difference between the Gibbs free energy of formation ($\Delta G_{fi,T}^0$) for products and reactants (Eq. (5)).

$$K_{rxn,T} = \exp\left(\frac{-\Delta G_{rxn,T}^0}{RT}\right) \quad (4)$$

$$\Delta G_{rxn,T}^0 = \sum v_i \Delta G_{fi,T}^0 \quad (5)$$

Furthermore, the change of the Gibbs free energy of formation ($\Delta G_{fi,T}^0$) of various species as a function of the temperature was determined by the modified Franklin's correlation (Eq. (6)), developed by van Krevelen and Chermín (1951). Franklin's method considers that molecules are formed by different groups of atoms with these groups all contributing to the property under consideration. This approach also introduces corrections for molecule symmetry (σ), and molecular form (Franklin, 1949). Franklin's method allows determining contribution values for specific temperatures, while the modified Franklin's correlation (Eq. (6)) considers group contributions changing linearly with temperature (van Krevelen and Chermín, 1951). Deviations between calculated and experimental ΔG_{fi}^0 at 298 K, when

available, were lower than 6.5%.

$$\Delta G_{fi,T}^0 = \sum N_j \left[A_j + \frac{B_j}{100} T \right] + RT \ln \sigma + \sum_{\substack{\text{corrections} \\ \text{if necessary}}} \quad (6)$$

Equilibrium constants for thiophene conversion over zeolites are reported in Figs. 6–9. On this basis, it can be observed that under conditions where there is no an external hydrogen source or a co-reactant, reactions 1, 5 and 14 are the only ones contributing, with reaction 5 being the thermodynamically favored. As shown in Fig. 6, thiophene conversion to benzothiophene (reaction 5) is almost irreversible, with an equilibrium constant between 4×10^4 and 8×10^5 , whereas reactions 1 and 14 involve equilibrium constants lower than 10^{-6} . Thus, production of butadiyne (reaction 1) and dimerization of thiophene (reaction 14) seem, under these conditions, unlikely to happen, while benzothiophene and H_2S appear being the favored products in the absence of a hydrogen donor.

In presence of a hydrogen donor, thiophene conversion involves a number of other competitive reactions (reactions 2, 3, 4 and 6 reported in Fig. 7). Under the studied conditions, the equilibrium constants for reaction 4 are consistently much higher than the ones for reactions 2 and 3. On the other hand, thiophene hydrogenation (reaction 6), with an equilibrium constant lower than 10^{-8} , is not

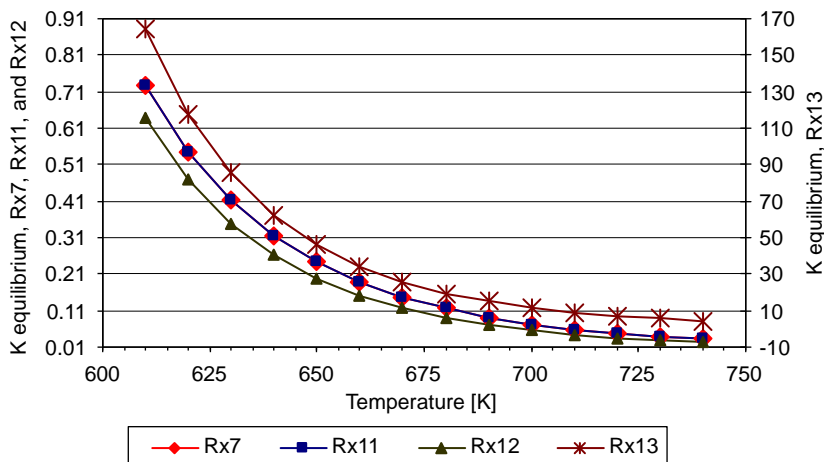


Fig. 8. Influence of temperature on thermodynamic equilibrium constants for thiophene alkylation reactions (reactions 7, 11, 12, and 13).

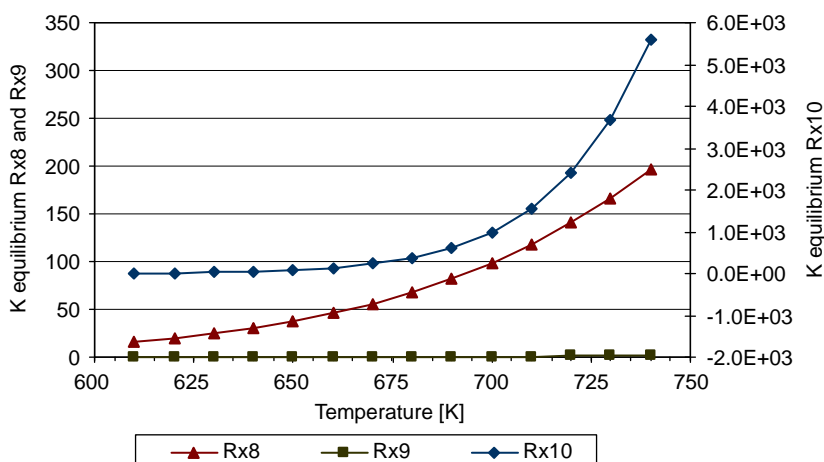


Fig. 9. Temperature influence on the thermodynamic equilibrium constants for thiophene alkylation/dealkylation and cyclization of alkyl-thiophenes (reactions 8, 9, and 10).

thermodynamically allowed. As a result, in presence of a hydrogen donor and under the conditions evaluated, the most thermodynamically favored products from thiophene conversion are benzene, ethylene, and H_2S .

Thiophene may also react under the presence of alkenes. The equilibrium constants for reactions 7, 11, 12 and 13, show that alkylation is a thermodynamically allowed reaction being favored with the alkyl chain length reduction (see Fig. 8). Additionally, alkylation reactions display higher equilibrium constants than other reactions also involving alkyl-thiophene formation (reaction 3). Thus alkyl-thiophenes formation seems more thermodynamically favored through alkylation reactions than thiophene ring opening with hydrogen transfer.

In order to fully assess the possible reaction steps, the cracking of alkyl-thiophenes (reactions 8 and 9) or cyclization of them (reaction 10) were also evaluated (see Fig. 9). The equilibrium constants of butyl-thiophene cyclization show the highest values ($8 < K_{Rx10} < 8400$). On the other hand, it was also observed via thermodynamic analysis that the cracking reaction of butyl thiophene leading to methyl thiophene and propylene ($15 < K_{Rx8} < 230$), is a preferred step versus the one yielding ethyl thiophene and ethylene ($0.07 < K_{Rx9} < 1.7$). As a conclusion, if a long alkyl-thiophene is produced, cyclization is more likely to happen than side group cracking.

Once the equilibrium for thiophene calculated, the reactions with equilibrium constants lower than 10^{-6} were neglected, with this including reactions 1, 2, 6 and 14. Additionally, cyclization of butenyl thiophene was the only reaction retained for butenyl thiophene with the side cracking reactions (reactions 8 and 9) being ignored.

To calculate the equilibrium conversion of thiophene a mixture of 5 wt% of thiophene and 95 wt% of *n*-octane was used, being *n*-octane both hydrogen donor and olefins source. In this manner, the catalytic cracking of *n*-octane leading to olefins (ethylene, 1-butene and propylene) was added to the thiophene reaction network.

Taking into account all the mentioned above considerations, a matrix of independent reactions was established. One can notice that the equilibrium conversion of thiophene becomes close to 100% in the 610–740 K range with reactions 4, 5, 8, 10 and 13 displaying equilibrium constants larger than 1.

In summary, the thermodynamic analysis is valuable to demonstrate the following: (a) thiophene conversion is not thermodynamically constrained, (b) alkylation reactions are favored over hydrogen transfer reactions, (c) thiophene conversion likely produces H_2S , benzene, methyl-thiophene, ethyl-thiophene and benzothiophene, being the later the preferred product, and (d) butadiene, tetra-hydro-thiophene, and thiophene dimers are species likely not to be formed.

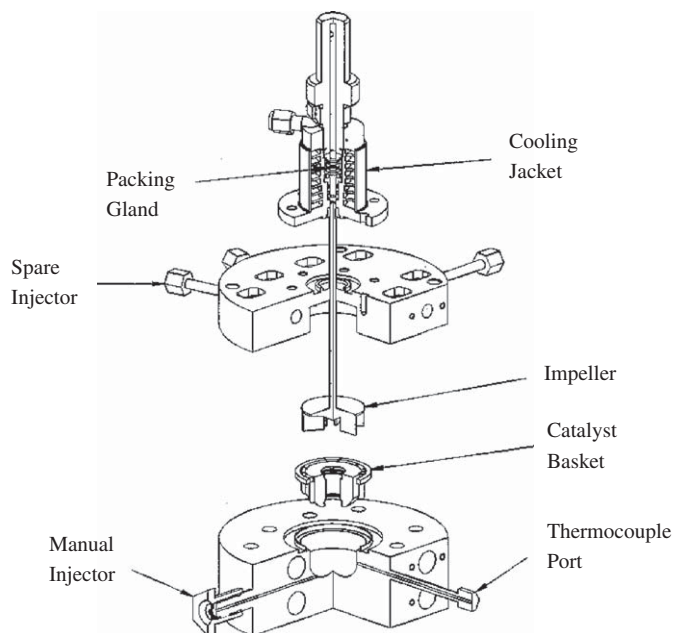


Fig. 10. Schematic diagram of the CREC riser simulator: quarter section view, upper and lower shells exploded.

3. Experimental

3.1. Catalyst and materials

A commercial catalyst from Albermale with the Z-2 code was used in this research. This catalyst was considered given its high content of H-ZSM5 supported in an inner matrix. Physical chemical characterization of Z-2 catalyst included particle size distribution (PSD), average bulk density (ABD), X-ray Diffraction (XRD), Electron Probe Microanalysis (EPMA), Temperature Programmed Desorption (TPD), surface area (BET and T-Plot), and Fourier transform infrared spectroscopy (FTIR). Additionally, H-ZSM5 synthesized in CREC laboratories (de Lasa et al., 2006) was used as a reference for zeolite characterization.

A model compound, thiophene C_4H_4S (Aldrich 99% purity), was selected as sulfur key specie in gasoline, with gasoline being simulated with *n*-octane (Aldrich 99% purity), a straight-chain hydrocarbon with a boiling point falling in the middle of the gasoline boiling range.

3.2. Reaction system

Experiments were developed using the CREC (Chemical Reactor Engineering Center) fluidized riser simulator (de Lasa, 1992). The CREC "Riser Simulator" is a bench scale mini-fluidized bed unit with 50 cm^3 and 1 g of catalyst capacity, that mimics the operating conditions of an industrial unit in terms of reaction time, temperature, hydrocarbon partial pressures and catalyst/oil ratios, allowing the testing and development of new catalysts.

A schematic diagram of a CREC Riser Simulator is reported in Fig. 10 (de Lasa, 1992). An impeller located in the upper section and a basket containing the catalyst placed in the central section, are the main components. Upon rotation of the impeller, gas is forced downwards in the outer reactor annulus. This creates a lower pressure in the central region of the impeller with a spiraling upwards flow of gas in the catalyst chamber. Two porous plates keep the catalyst inside the central chamber under high fluidization conditions. The Riser Simulator operates in conjunction with a vacuum box and

series of valves that allow, following a predetermined sequence, to sample hydrocarbons and withdraw products from the CREC Riser Simulator in short periods of time.

The Fig. 11 shows a schematic description of the CREC riser simulator and associated valves and accessories. Applications of the CREC Riser Simulator to catalytic cracking have been widely reported, excellent examples are the studies conducted at CREC on FCC catalysts (Atias et al., 2003) and the evaluation of zeolites as desulfurization catalyst (de Lasa et al., 2006).

Regarding the application of the CREC Riser Simulator to the present study, it is important to mention that this unit is particularly well equipped for mechanistic studies. The sample collected in the vacuum box at vacuum pressure (e.g. 3 psia) provides information about the combined abundance of species both in the gas and in the catalyst phases. This combined measurement is essential to argue about species formed in a catalytic reaction network such as the one of this study.

3.3. Experimental procedure

Thermal and catalytic runs were performed in the above-described reactor. Mixtures of thiophene and *n*-octane were reacted at atmosphere pressure, mild temperature (350, 375, 400, 425, and 450°C), contact times 5, 10, 15, and 20 s, and different concentrations of thiophene (0–6 wt%). The maximum reaction time (20 s) was selected after preliminary runs to minimize catalytic cracking of *n*-octane, and the maximum temperature (450°C) was chosen to diminish the thermal cracking of both thiophene and *n*-octane. The catalyst to oil ratio (cat/oil) was set at 5 and the impeller velocity at 5600 rpm to get a well fluidized bed.

The Z-2 catalyst already thermally treated in Albermarle was further calcined in CREC riser simulator at 550°C under air flow for 25 min. The pre-treated catalyst was loaded in the catalyst basket, the reaction system was sealed, leak tested and heated to the reaction temperature in argon atmosphere. Then, the reactant mixture was injected, and once the reaction time was reached, the reaction products were evacuated from the reactor and sent to the analytical system, through a heated transfer line. All experiments were repeated at least 3 times to secure reproducibility of results.

3.4. Analytical system. identification and quantification of products

An Agilent 5973N mass selective detector (MSD) was used to identify the reaction products, while An Agilent 6890N gas chromatograph (GC) with flame photometric detector (FPD) and flame ionization detector (FID) allowed the quantification of them. The FPD was utilized for the selective detection of sulfur compounds at ppm levels in hydrocarbon mixtures, with calibration curves that correlate calculated areas and concentrations of sulfur in hydrocarbon mixtures developed prior to the experimental runs. In addition, the FID was employed to quantify the hydrocarbon species in a sulfur free basis. Two HP-1 Dimethylpolysiloxane capillary columns with a length of 50 m, a nominal diameter of 0.50 mm, and a nominal film thickness of $0.5\ \mu\text{m}$ permitted the separation of the components present in the samples. Both columns were connected to the back inlet of the GC. While one of the column ends was linked to an MSD, the other one was split and coupled to both FID and FPD detectors. In this way, each single injection produced three signals, one per detector, with this detector configuration allowing identification and quantification of various hydrocarbon products as well as sulfur species in hydrocarbons mixtures with low sulfur content.

The GC oven program was run using the following thermal ramp: (a) initially the oven temperature was set at 308 K for 10 min, (b) following this, the temperature was increased at 8 K min^{-1} up to 343 K, (c) once 343 K was reached, the temperature was raised at

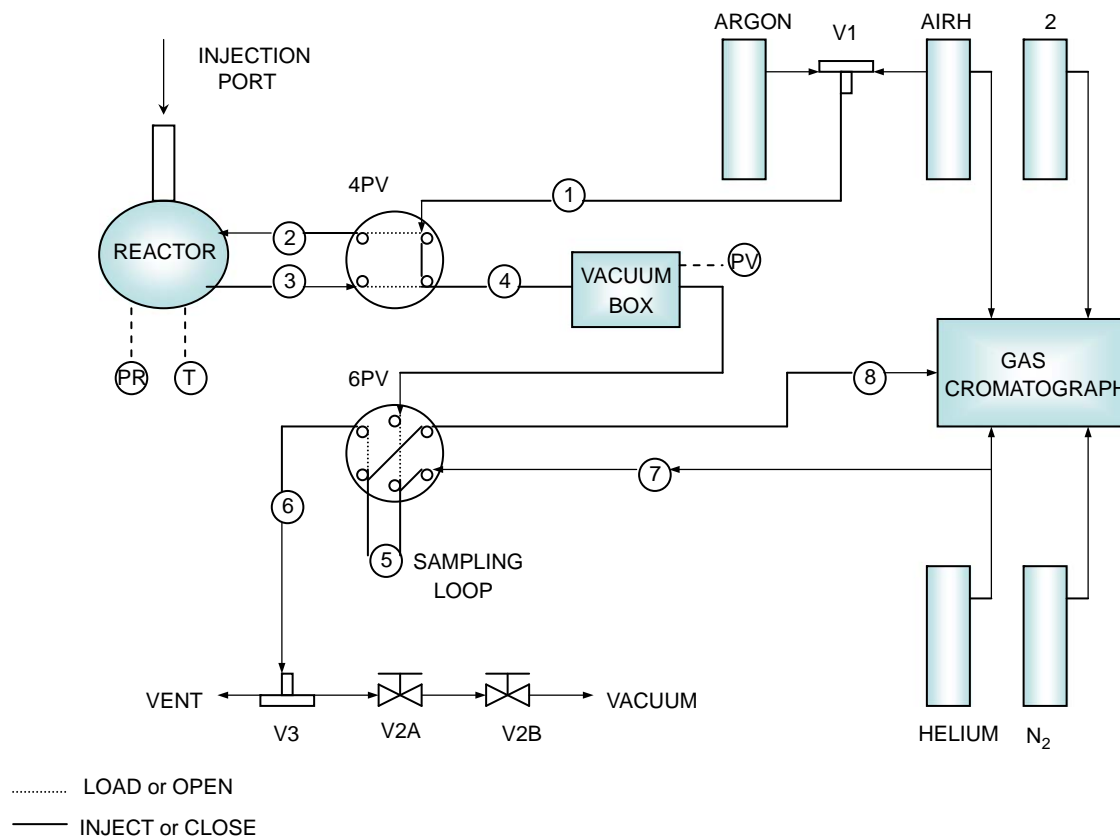


Fig. 11. Schematic description of CREC riser simulator, associated valves and accessories.

15 K min⁻¹ up to 573 K, and (d) finally, at 573 K the temperature was hold for 10 min.

3.5. Recovery and identification of compounds retained on the catalyst

Total coke over catalyst was measured in a total organic carbon analyzer (TOC-V) with a solid sample module (SSM-5000) from Mandel. In addition, Guisnet and Magnoux's (1989) method was used to recover the compounds retained on coke: dissolution of the catalyst in a 40% hydrofluoric acid (HF) solution followed by extraction of organic compounds by methylene chloride (CH₂Cl₂). After removal of the solvent, species forming the coke were identified using the GC/MSD system described in Section 3.4.

4. Results and discussion

4.1. Catalyst characterization

The PSD of the Z-2 catalyst sample was measured using a Mastersizer 2000 from Malvern Instruments. The average particle size was assessed at 84 μm, with the 0–20 and 0–40 μm catalyst fractions being limited to 10 and 19 vol%, respectively. This limited fraction of fines prevented plugging of the reactor porous plates. The apparent density of the catalyst was assessed at 1535 kg m⁻³ using a method established at CREC.

The gas density for pure *n*-octane at 200 kPa and 400 °C was assessed at 0.245 kg m⁻³. Using this parameter, the average particle size, the particle apparent density and Geldart's (1973) powder classification chart, it was concluded that the Z-2 catalyst particles belong to the group A, a particle group considered to display good fluidization.

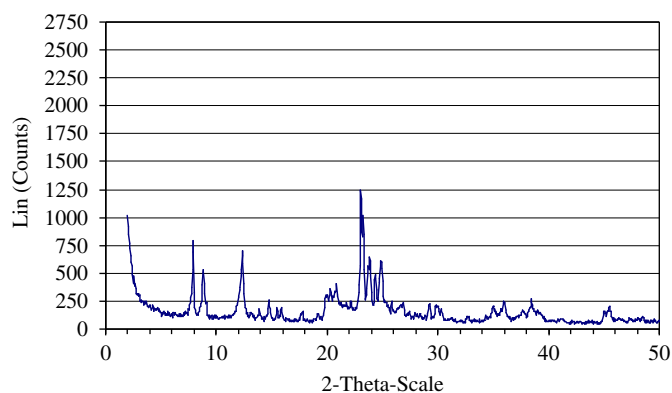


Fig. 12. X-ray diffraction of Z-2 catalyst.

XRD was used to confirm the presence of H-ZSM5 zeolite in the Z-2 catalyst sample. The XRD analysis was performed using Cu-K α radiation in a rotating anode X-ray diffractometer over a 2θ range from 2° to 82° (Figs. 12 and 13). One can notice that XRD patterns display peaks in close 2θ values, confirming that the crystals in the Z-2 catalyst are indeed those of H-ZSM5 zeolite. Comparison of the characteristic peak at 23.6 shows a XRD peak relationship close to the zeolite/matrix as reported by Albermarle, with 49.7% crystallinity as assessed with XRD.

The chemical composition of the Z-2 catalyst was measured using EPMA. Prior to the EPMA analysis, the catalyst sample was prepared in the form of a metallographically polished bulk solid. It was shown that Si/Al ratio for this catalyst was 3.46 with a low sodium content of 0.08 wt%.

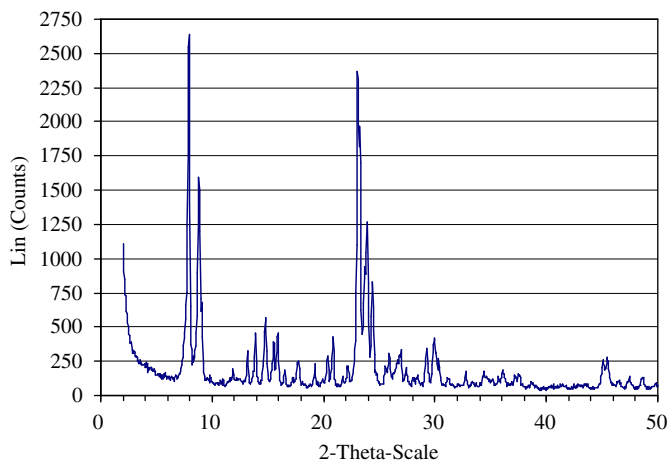


Fig. 13. X-ray diffraction of H-ZSM5 reference zeolite.

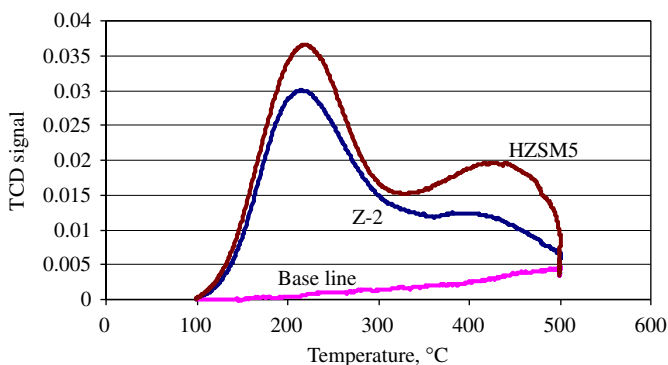


Fig. 14. TPD spectrums of Z-2 catalyst and H-ZSM5 reference zeolite.

TPD experiments were performed using an AutoChem II analyzer from Micromeritics. A 0.172 g, sample was pretreated by a helium purge for 2 h at 500 °C. Ammonia was adsorbed for 1 h at 100 °C using an NH₃/He gas mixture (4.52% ammonia, 95.58% helium). After dosing, the sample was purged in He for 1 h at the adsorption temperature. During the TPD experiments, the temperature of the sample was increased linearly by 15 °C min⁻¹ until 500 °C in flowing helium. Ammonia TPD for both the Z-2 catalyst and H-ZSM5 zeolite are reported in Fig. 14. Deviations of Z-2 catalyst acidity under pretreatment conditions, as described in Section 3.3, were smaller than 8%.

TPD spectra displays two consistent desorption peaks centered at 220 and 430 °C, confirming that both Z-2 catalyst and H-ZSM5 zeolite contain weak acidic sites and strong acidic sites. Furthermore, total acidity for both Z-2 catalyst and H-ZSM5 zeolite were determined by integrating the TPD spectrums (Fig. 14). Z-2 catalyst displayed an acidity of 0.048 mmol NH₃ g⁻¹ while H-ZSM5 reference zeolite showed a higher 0.063 mmol NH₃ g⁻¹ value, an expected difference given the catalyst under study is mainly H-ZSM5 zeolite dispersed in a silica-kaolin matrix.

The specific surface of the Z-2 catalyst was measured using an ASAP 2010 analyzer (from Micromeritics). Before the measurements, samples weighing from 0.15 to 0.2 g were degassed at 643 K for 4 h. Adsorption isotherms were measured under the relative pressure range from $\sim 10^{-6}$ to 1. The total Z-2 catalyst surface area (BET) observed was 92 m² g⁻¹ with the zeolite (micropore) after the T-plot calculations contributing with 71 m² g⁻¹ while the matrix with 21 m² g⁻¹.

On the basis of the Z-2 catalyst characterization, it is possible to conclude that: (a) the physical properties of the catalyst particles are adequate for good fluidization, (b) the catalyst presents both weak and strong acid sites, and (c) XRD, TPD and surface area of catalyst confirm a high concentration of H-ZSM5 zeolite, the main component accounting for catalytic activity.

4.2. Thiophene conversion over Z-2 catalyst

Thermal runs under the most severe conditions, without catalyst being loaded in the reactor, were initially developed to determine possible thermal cracking of both thiophene and *n*-octane. While no thiophene conversion was observed at 450 °C and 20 s, *n*-octane reported a small conversion of 0.44%. Therefore, thermal cracking was neglected under the conditions studied, and the conversion observed during the catalytic runs (catalyst loaded) truly represents the H-ZSM5 catalytic effects.

4.2.1. Thiophene conversion and products distribution

Catalytic runs with thiophene and *n*-octane mixtures were performed at cat/oil of 5, mild temperatures (350, 375, 400, 425, and 450 °C), and reaction times of 5, 10, 15, and 20 s. A typical set of data is included in the present work in Table 1, and Appendix A. As described in Section 3.4, the products distribution in gas phase was determined with combined GC/MSD system. The FID and FPD signals are reported in Figs. 15 and 16.

On the basis of these mass spectra, the peaks in Figs. 15 and 16 were assigned to the products listed in Table 1 and Appendix A.

One can observe in Table 1, that the converted *n*-octane produced mainly light olefins (ethylene, propylene, and, butene's), isobutane and, *n*-butane, with these species representing a typical product distribution of *n*-octane catalytic cracking over H-ZSM5 zeolites (Smirniotis and Ruckenstein, 1994).

A decrease of thiophene in the hydrocarbon product stream was observed for mixtures with less than 1 wt% (0.77 wt% Argon basis). This reduction in thiophene concentration with no other sulfur species present in the product stream (see Table 1), was assigned to the possible contribution of thiophene adsorption. These findings are in agreement with data reported by Richardeau et al. (2004), who also observed that there was no thiophene conversion in thiophene-*n*-heptane mixtures at concentrations of thiophene lower than 0.3 wt%.

Regarding the catalytic conversion of thiophene in the presence of *n*-octane main sulfur products were: H₂S, alkyl-thiophenes, benzothiophene, and coke. No tetra-hydro-thiophene was found either at several initial thiophene concentrations (Table 1) or at different reaction temperatures and reaction times (Appendix A, Tables A1 and A2). This finding is in agreement with the thermodynamic analysis, where the hydrogenation of thiophene (reaction 6, Fig. 1) is thermodynamically constrained under the temperature range studied (350–450 °C).

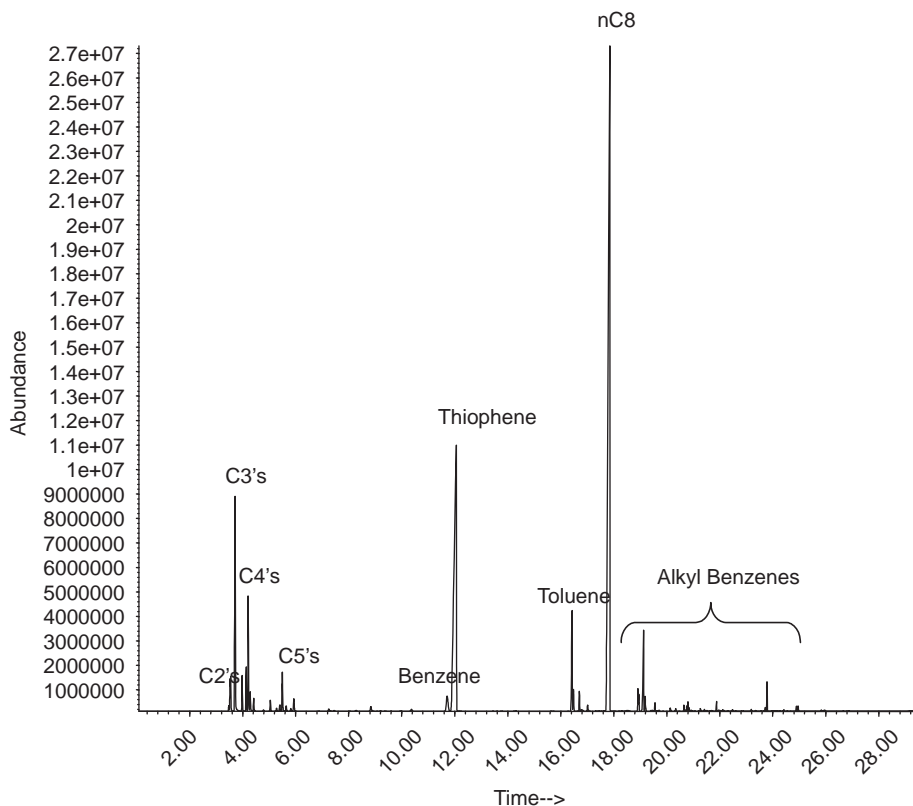
It can also be noticed in Table 1, that the production of aromatics such as toluene, and alkyl-benzenes increased at higher concentrations of thiophene. This was attributed to the contribution of thiophene conversion via reaction 4 (Fig. 1) followed by quick alkylation of benzene. Conversion of thiophene to aromatics products was as well reported by Li et al. (2001). One should also mention that in spite of the fact that benzene was observed in the MSD, its concentration in the product stream could not be adequately quantified using GC/FID in the samples with less than 10 wt% of thiophene.

Furthermore, and under all the reaction conditions studied, the production of H₂S confirms the contribution of thiophene conversion via reactions involving thiophene ring opening and hydrogen transfer. The influence of thiophene alkylation reactions were also apparent given the following: (a) reduction of light olefins with

Table 1Conversion and products distribution from catalytic conversion of thiophene/*n*-octane mixtures at 450 °C, reaction time 20 s, and catalyst/feedstock = 5.

Reactant mixture								
Th (wt%)	0.00	0.38	0.99	1.88	2.76	4.52	5.27	6.23
<i>n</i> C ₈ (wt%)	100.00	99.62	99.01	98.12	97.24	95.48	94.73	93.77
Hydrocarbon products distribution (wt%)								
C ₂ 's	1.47	1.43	1.40	1.56	1.60	1.60	1.57	1.46
C ₃ 's	11.68	11.62	11.68	11.79	11.78	10.62	10.48	10.28
isoC ₄	2.98	2.98	2.95	2.99	2.93	2.77	2.58	2.50
<i>n</i> C ₄	4.49	4.70	4.61	4.60	4.40	4.38	4.36	4.30
C ₄ =	3.14	3.06	3.05	2.81	2.49	2.44	2.35	2.18
C ₅	3.20	3.08	2.95	2.53	2.44	2.38	2.35	2.23
C ₅ =	1.36	1.36	1.32	1.28	1.20	1.20	1.16	1.09
<i>n</i> C ₈	69.69	69.62	69.00	68.76	68.65	68.73	68.59	68.48
Toluene	1.21	1.02	1.27	1.31	1.34	1.42	1.52	1.70
Alkylbenzene	0.77	0.77	1.01	1.00	1.17	1.39	1.40	1.50
Sulfur products distribution (ppm)								
H ₂ S		0	0	0	22	126	333	516
Thiophene (wt%)		0.38	0.76	1.37	2.00	2.99	3.38	3.95
Methyl thiophene		0	0	32	39	370	994	1221
Ethyl thiophene		0	0	20	26	202	686	754
2-(1Methyl ethyl) thiophene		0	0	0	0	11	315	440
2-Propyl thiophene		0	0	0	0	16	177	230
2-Butyl thiophene		0	0	0	0	0	43	50
Benzothiophene		0	0	0	0	16	31	79
Methyl benzothiophene		0	0	0	0	0	0	8
H ₂ S/(alkyl-Th+benzo-Th) ^a		0	0	0	0.95	0.63	0.47	0.59
Coke (%) (wt coke/wt cat)	0.04	0.04	0.04	0.05	0.05	0.07	0.07	0.07
<i>n</i> -Octane conversion (%)	30.45	30.26	30.45	30.10	29.58	28.26	27.84	27.23
Thiophene conversion (%)	N/A	0.20	23.62	27.53	27.89	34.08	36.03	36.85
Thiophene selectivity (S _{Th})	N/A	2	78	48	33	25	23	20

Species reported are the result of combination of gas phase products and adsorbed species at the evacuation reaction time.

^aMole ratio.**Fig. 15.** FID signal of hydrocarbon products in gas phase from thiophene/*n*-octane conversion at 450 °C, reaction time 20 s, catalyst/feedstock = 5.

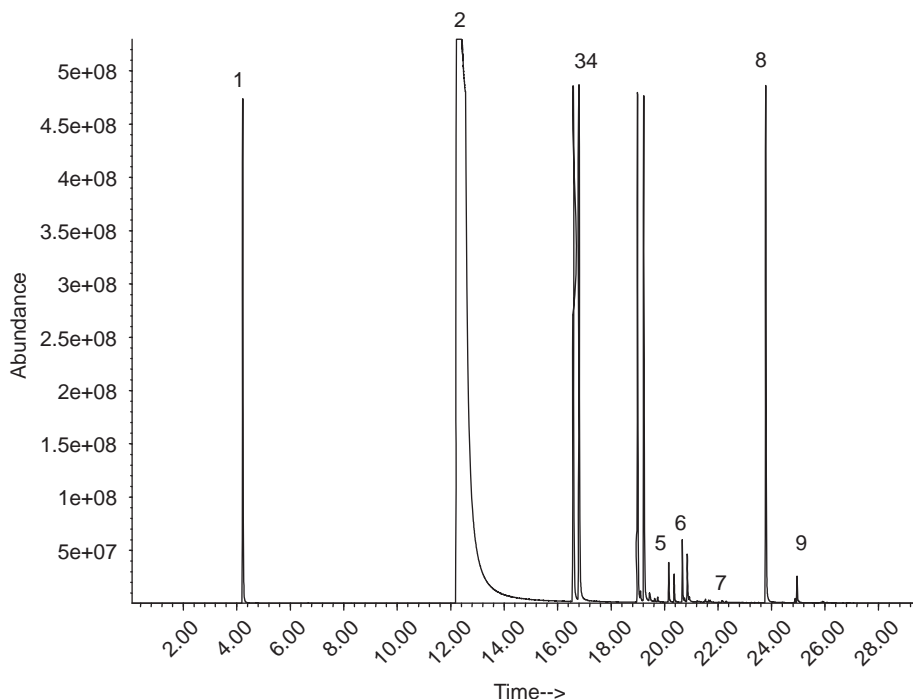


Fig. 16. FPD signal of sulfur compounds in hydrocarbon product stream from thiophene/*n*-octane conversion at 450 °C, reaction time 20 s, catalyst/feedstock = 5: (1) H₂S, (2) thiophene, (3) methyl-thiophene, (4) ethyl-thiophene, (5) methyl-ethyl-thiophene, (6) propyl-thiophene, (7) butyl-thiophene, (8) benzothiophene, and (9) methyl-benzothiophene.

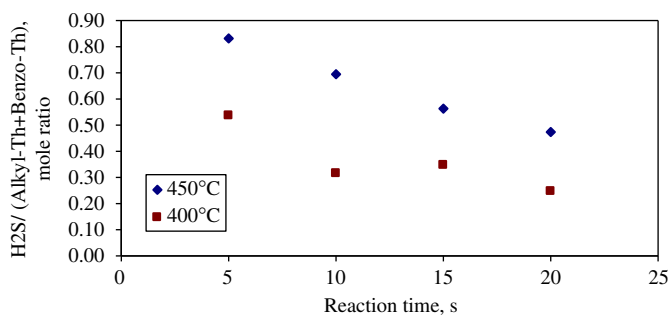


Fig. 17. H₂S/(alkyl-thiophenes+benzothiophene) mole ratio from catalytic conversion of thiophene/*n*-octane mixtures, 5 wt% thiophene, cat/oil = 5, reaction times 5, 10, 15, and 20 s, and reaction temperatures 400 and 450 °C.

progressive alkyl-thiophenes formation, (b) observed H₂S/(alkyl-thiophenes+benzothiophene) mole ratio lower than unity, and (c) production of methyl-benzothiophene and formation of thiophenes with multiple-alkylated groups such as 2-(1-methylethyl)thiophene.

Fig. 17, with further details provided in Tables A1 and A2 of the manuscript's Appendix A, shows the characteristic and consistent mechanistic patterns at two temperatures and four residence times (5, 10, 15, and 20 s), as follow:

- H₂S/(alkyl-thiophenes+benzothiophene) mole ratio decreases with the reaction time, although alkyl-thiophene, benzothiophene and H₂S production consistently increases (refer to Tables A1 and A2). This can be assigned to the higher olefin availability for thiophene alkylation reactions due to the increased *n*-octane conversion with the reaction time.
- H₂S/(alkyl-thiophenes+benzothiophene) mole ratio is higher in the catalytic runs at 450 °C. This increment of the H₂S selectivity with the reaction temperature can be explained consid-

ering that reactions that involve thiophene ring opening and hydrogen transfer are endothermic and as a result one can argue that these reaction are thermodynamically favored at higher temperatures.

Regarding alkylation, it was observed in Tables 1, A1, and A2, that the relative distribution of alkyl-thiophenes formed was in agreement with the thermodynamic predictions, with the alkylated species abundance following the sequence: C₁ thiophene > C₂ thiophene > C₃ thiophenes > C₄ thiophene. Moreover, the yield of butyl-thiophene was significantly lower than the one for other alkyl-thiophenes. This special trend was assigned to side chains cyclization and cracking, with cyclization being the preferred pathway as predicted by thermodynamics (see reactions 8, 9 and 10, Fig. 2).

In the present study, and in order to be able to assess the competitive changes of thiophene and *n*-octane, a conversion selectivity parameter is considered as follows:

$$S_{\text{Th}} = \frac{X_{\text{Th}}/W_{\text{Th}}}{X_{n\text{C}_8}/W_{n\text{C}_8}} \quad (7)$$

where X_{Th} and $X_{n\text{C}_8}$ are the thiophene and *n*-octane conversion based on W_{Th} and $W_{n\text{C}_8}$, the masses of thiophene and *n*-octane injected as reactants.

This selectivity parameter lumps the combined effects of adsorption and reaction surpassing the value of 1 in all cases (refer to Tables 1, A1 and A2). This confirms the greater adsorption affinity of thiophene versus *n*-octane or alternatively a much higher intrinsic rate of thiophene dehydrosulfidation compared to the hydrocarbon cracking rate. This is a relevant property given the significant differences in gas-phase concentrations between hydrocarbon and thiophene. These results are consistent with those reported by Chica et al. (2005).

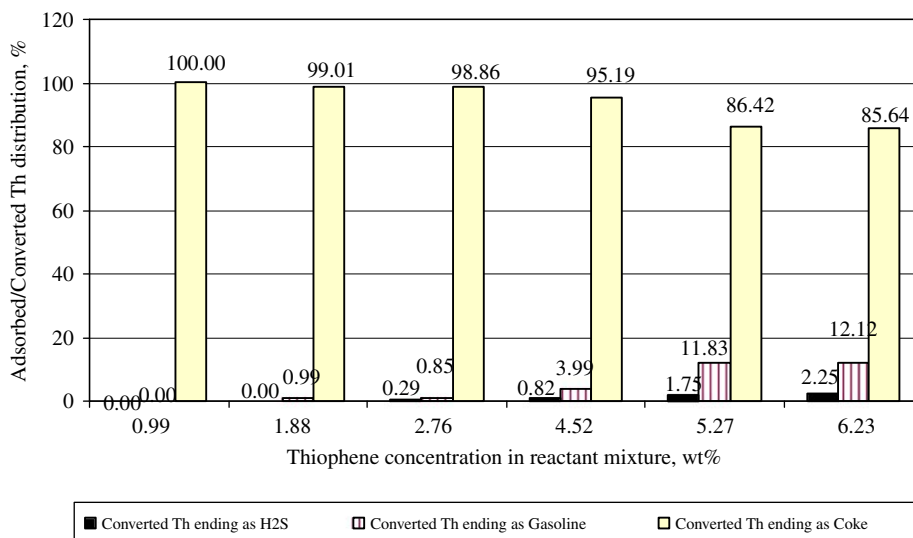


Fig. 18. Converted thiophene distribution in process streams (gas, gasoline and coke). Reaction conditions: 450 °C, 20 s, catalyst/feedstock = 5.

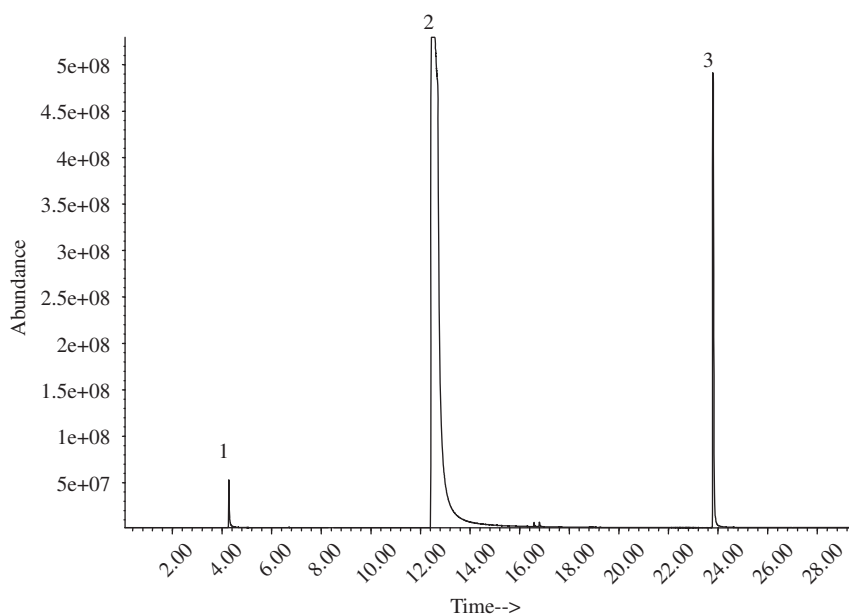


Fig. 19. FPD signal of sulfur compounds in hydrocarbon product stream from pure thiophene conversion at 450 °C, 20 s, catalyst/feedstock = 5: (1) H₂S, (2) thiophene, and (3) benzothiophene.

4.2.2. Distribution of converted thiophene in product streams

The fraction of converted thiophene distributed in process streams (gas, gasoline, and coke) was determined using the Gas_{cTh} , $Gasoline_{cTh}$ and $Coke_{cTh}$ parameters as follows:

$$(a) \quad Gas_{cTh} = \frac{W_{H_2S}}{X_{Th}W_{Th}} \times 100 \quad (8)$$

with Gas_{cTh} being the percentage of converted thiophene ending in a gas process stream, W_{H_2S} the mass fraction of H₂S in the product, W_{Th} the mass fraction of thiophene in the reactant mixture, and X_{Th} the conversion of thiophene.

$$(b) \quad Gasoline_{cTh} = \frac{\sum W_i}{X_{Th}W_{Th}} \times 100 \quad (9)$$

with $Gasoline_{cTh}$ representing the percentage of converted thiophene ending in C₅–C₁₂ fraction and W_i the concentration of the sulfur species that fall into the C₅–C₁₂ boiling point range, such as alkylthiophenes, benzothiophene and methyl-benzothiophene.

$$(c) \quad Coke_{cTh} = 100 - Gas_{cTh} - Gasoline_{cTh} \quad (10)$$

with $Coke_{cTh}$ being the percentage of converted thiophene in coke.

Fig. 18 reports the distribution for fractions of adsorbed/converted thiophene in process streams: gas, gasoline and coke. On the basis of this data, it can be observed that in all cases more than 85% of the adsorbed/converted thiophene ends over the catalyst as coke. Even more one can notice that at the lowest thiophene concentrations (e.g. 1 wt%) the entire sulfur product species from thiophene remain undetected at the reactor exit. However, when thiophene concentration is increased in the reactant mixture, one can then

detect sulfur product species with boiling points in the C₁–C₄ range (gas) and in the C₅–C₁₂ range (gasoline). This phenomenon is probably due that at the higher thiophene concentrations there is an increased tendency of prompting bimolecular reaction involving ring opening and hydrogen transfer.

Taking into consideration the above it can be concluded that adsorption as well as reaction of gasoline sulfur species over zeolites leads to significant coke levels. As a result, such as catalytic desulfurization should involve both a reactor and regenerator for having a process operating a high level of catalyst activity.

4.2.3. Influence a hydrogen donor in thiophene conversion over H-ZSM5 zeolites

In order to evaluate the influence of a hydrogen donor in the thiophene conversion, catalytic runs with pure thiophene and

Table 2

Influence of an external source of hydrogen in thiophene conversion, at 450 °C, 20 s, catalyst/feedstock = 5.

Reactant mixture (wt%)^a		
Th	42	100
nC ₈	58	0
Reactant mixture (wt%)^b		
Th	27.48	26.93
nC ₈	37.94	0.00
Ar	34.58	73.07
Sulfur products distribution (wt%)^c		
H ₂ S	2.73	0.09
Thiophene	27.49	97.61
C ₁ thiophene	4.32	0.00
C ₂ thiophene	3.47	0.00
C ₃ thiophene	0.76	0.00
C ₄ thiophene	0.06	0.00
Benzothiophene	2.01	2.30
C ₁ benzothiophene	0.10	0.00
Coke over catalyst (wt%) (wt coke/wt catalyst)	0.21	0.38
Conversion nC ₈ (%)	13.90	N/A
Conversion Th (%)	35.19	11.38
Converted Th ending in gas (as H ₂ S) (%)	18.47	0.76
Converted Th ending in gasoline (%)	72.58	20.23
Converted Th ending in coke (%)	8.95	79.01

^aSample injected to the reactor.

^bReactant mixture into the reactor under argon atmosphere at reaction conditions (P,T).

^cArgon free basis.

thiophene/*n*-octane mixture, under same reaction conditions (450 °C, 20 s, catalyst/feedstock = 5) and thiophene concentration (27 wt% argon basis), were carried out. For the catalytic runs with pure thiophene, the amount of sample injected into the reactor was reduced from 0.16 to 0.04 g, and the catalyst loaded from 0.8 to 0.2 g. This to provide the same catalyst to feedstock ratio, and thiophene partial pressure set in the runs with thiophene/*n*-octane. The FPD signal of pure thiophene cracking is shown in Fig. 19, and the product distribution in Table 2.

It can be noticed that in this case, the conversion of pure thiophene leads to benzothiophene and H₂S, probably through reaction 5 (Fig. 1), while no butadiyne is observed. These results are consistent with the thermodynamic analysis (refer to Section 2), where production of butadiyne (reaction 1, Fig. 1) is limited, and thiophene conversion to benzothiophene (reaction 5, Fig. 1) is the preferred pathway in absence of a hydrogen donor.

On the other hand, it was found that conversion of thiophene was 3 times higher for thiophene/*n*-octane mixtures than pure thiophene, being this result in agreement to that reported by Iglesias's research group (Yu et al., 1999; Li et al., 2001; Chica et al., 2004). Moreover, it is confirmed in this study that in absence of a hydrogen donor there is much larger fraction of thiophene converted ending as coke (79.01% vs. 8.95%).

4.2.4. Sulfur species in coke

One key aspect on the development of a reaction mechanism for the catalytic gasoline dehydrodesulfidation is to be able to provide evidence that this conversion network takes place via adsorbed thiophene species. This important information is obtained, in the present study, from the GC/MSD analysis of the extracted compounds retained as coke. The TIC signal obtained from the coke extract is reported in Fig. 20, with the identity of sulfur products being assigned using the MSD spectra relative abundances (Table 3).

On this basis, it is found that the chemical species forming the coke include adsorbed thiophene, polyaromatics and heavy thiophenes, such as the ones reported in Table 3. It is important to point out that no thiophene dimer species were detected in the coke extract, with this finding being in agreement with the thermodynamic analysis of the present study.

Taking into consideration the critical molecular size of thiophene (5.4 Å), smaller than the pore zeolite opening (5.6 Å), one should not expect steric limitations in thiophene desorption. Thus, the adsorbed thiophene species found in coke, are most likely due to the irreversible or quasi irreversible adsorption of these basic molecules on

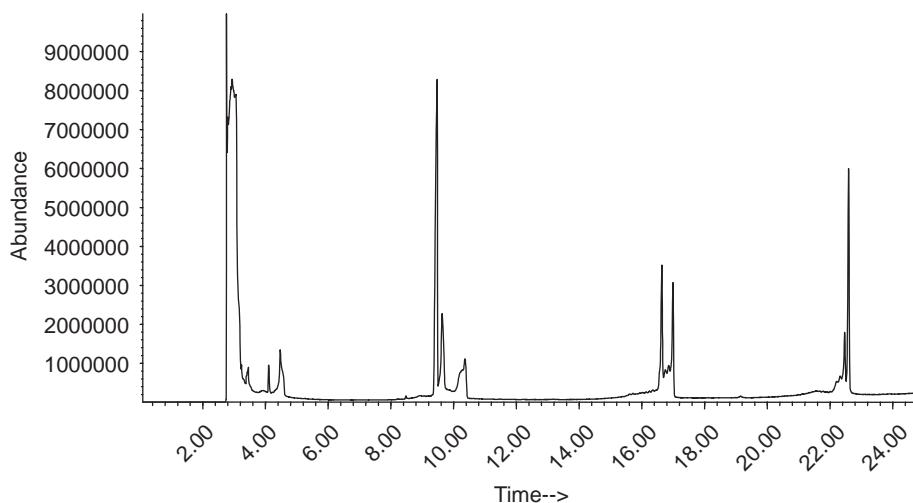
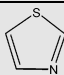
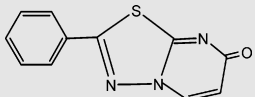
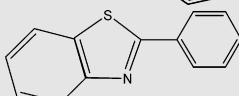
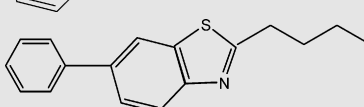
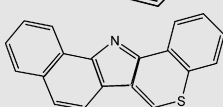
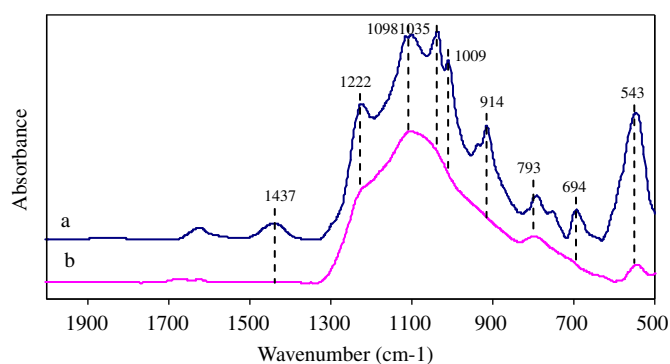


Fig. 20. TIC signal of compounds retained in H-ZSM5 after thiophene conversion from thiophene/*n*-octane mixtures, at 450 °C, 20 s, catalyst/feedstock = 5.

Table 3Main sulfur compounds retained in H-ZSM5 after thiophene conversion from thiophene/*n*-octane solution, at 450 °C, 20 s, catalyst/feedstock = 5.

Retention time (min)	Molecular weight (g mol ⁻¹)	General formula	Structure
2.76	85	C ₃ H ₃ SN	
9.64	229	C ₁₁ H ₇ SN ₃ O	
16.63	211	C ₁₃ H ₉ SN	
22.42	267	C ₁₇ H ₁₇ SN	
22.58	285	C ₁₉ H ₁₁ SN	

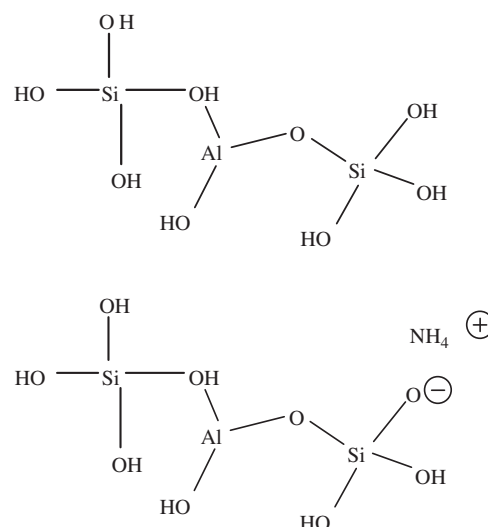
**Fig. 21.** FTIR spectra of: (a) Z-2 catalyst as received from Albermarle and (b) Z-2 catalyst further calcined at 500 °C for 8 h at CREC laboratories.

acid sites, as well as, the potential diffusivity hindrance effect on desorbed thiophene species by polyaromatics, resulting from oligomerization of *n*-octane catalytic products, and/or heavy thiophenic compounds.

Table 3 also reports heteroatomic polyaromatic species. These species include both nitrogen and sulfur atoms. Nitrogen in these extract coke species can likely be traced to the ammonia cations involved in the zeolite synthesis and still remaining on the Z-2 catalyst surface. In fact, in the ZSM5 preparation, there is a final ion exchange step where NO₃NH₄ removes the sodium from the Na⁺-ZSM5 structure. This step is followed by calcination and allows the ammonia to be released leaving the ZSM5 in its protonic acid form (H-ZSM5). However, if NH₄⁺ cations on the catalyst surface are not fully decomposed, ammonia cations can still remain on the surface partially covering catalyst sites. Even more, these ammonium cations can then facilitate the formation of heteroatomic polyaromatic species containing nitrogen as reported in Table 3.

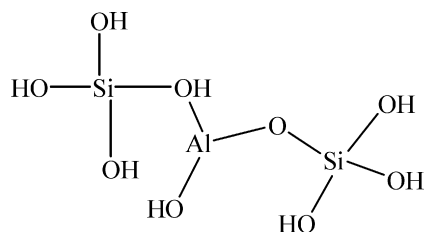
Fig. 21 reports the FTIR spectra for the Z-2 catalyst of the present study. Four of the IR bands observed (543, 793, 1098, and 1222 cm⁻¹) are characteristic of H-ZSM5 zeolites (Xu et al., 1995). The others at 1035 and 1009 cm⁻¹ correspond to Si–O–Si (plane vibrations) and finally the ones at 914 and 614 cm⁻¹ to the kaolin matrix filler (OH bending vibrations) (Deng et al., 2002).

The presence of NH₄⁺ cations on the catalyst surface after calcination was confirmed using the IR spectra (Fig. 21). In fact for the Z-2

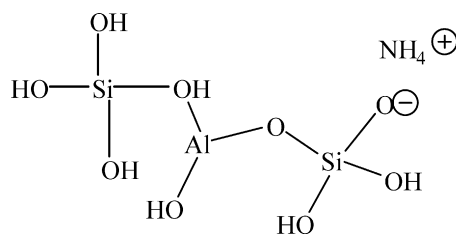
**Fig. 22.** Short model of adsorption site on ZSM-5 without residual NH₄⁺ (Scheme 1) and with residual NH₄⁺ (Scheme 2).

catalyst a 1437 cm⁻¹ band typically assigned NH₄⁺ (Xu et al., 1995) was observed. This band disappeared after heating the catalyst at 500 °C for 8 h.

The Z-2 catalyst sample was carefully heated in two steps: 120 °C for 1 h, ramp 1 °Cmin⁻¹, 500 °C for 8 h, ramp 2 °Cmin⁻¹. In spite of this, the FTIR spectrum of the calcined sample showed typical structural changes, due to the phase changes of kaolin, from crystalline to amorphous. Minor changes were also observed in the intensity of the 1222 cm⁻¹ band, an indication of a slight reduction of crystallinity.



Scheme 1.



Scheme 2.

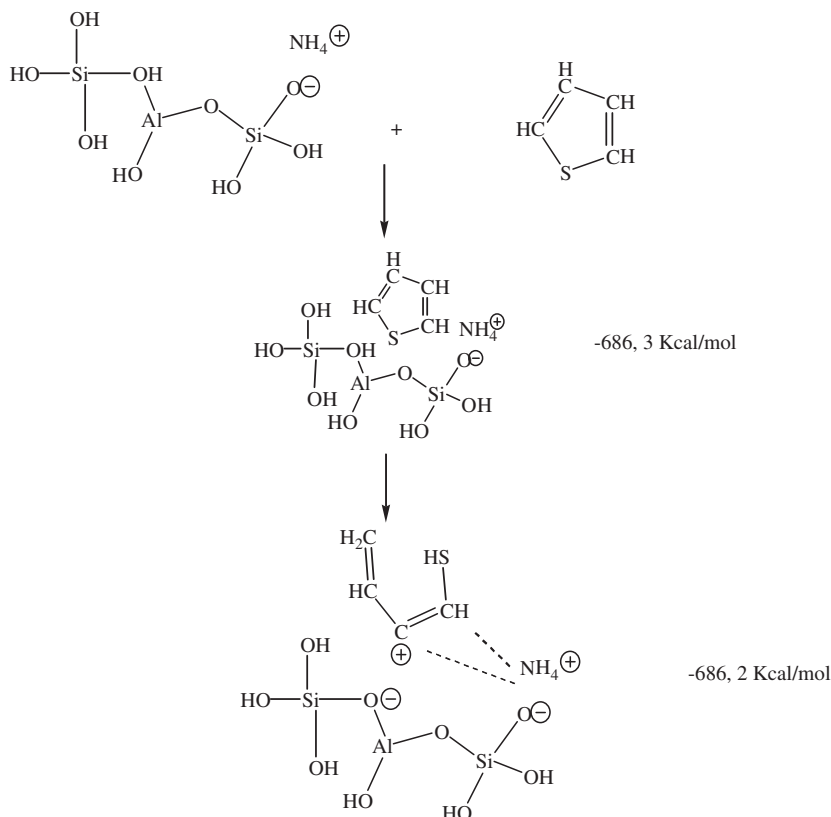


Fig. 23. Cationic thiophene species with positive charge on Carbon 3.

4.3. Modeling of thiazole formation

The nitrogen species found in coke (refer to Section 4.2.4) can be considered as evidence of the catalytic gasoline dehydrosulfidation via adsorbed thiophene species. In this sense, and to support this interpretation, the thiophene adsorption on a model of acidic site on the ZSM-5 zeolite is analyzed by MM2 structural minimization followed by a PM3 (parameterized model 3) minimization using the Chem3dUltra (Cambridge Soft). The MM2 minimization step is done to generate acceptable inputs for the semiempirical method PM3, with this method taking into account the electronics structure of the proposed model.

The structure of the selected simple string of the ZSM-5 zeolite is (OH)₃Si-O⁻H⁺-Al(OH)-O-Si(OH)₃. There are a Brønsted acidic site on the OH of the Si-OH-Al bond and a Basic Lewis site on the O of the Al-O-Si bond. Even more the OH from the Si-OH may be considered slightly Brønsted acidic and the OH on the Al a Brønsted basic (Fig. 22, Scheme 1).

Also the presence of ammonia bonded to the simple string of the zeolite structure is considered. It has been reported that H-ZSM5 retains the ammonia adsorbed above 400 °C (Bartholomew et al., 1997). The ammonium coordinated site is (OH)₃Si-O⁻H⁺-Al(OH)-O-Si(OH)₂O-NH₄⁺ (Fig. 22, Scheme 2); being the NH₄⁺ placed on a Si-O⁻ group, following the published literature on the topic (Elanaya et al., 2005).

4.3.1. Results of the molecular modeling calculation

Results of the molecular modeling calculations are presented in Figs. 23–26. The values included in the figures are formation energies (ΔH_f^0) for the individual conformation, calculated with the PM3 by minimization of the structure until a gradient norm of 0.1 is obtained.

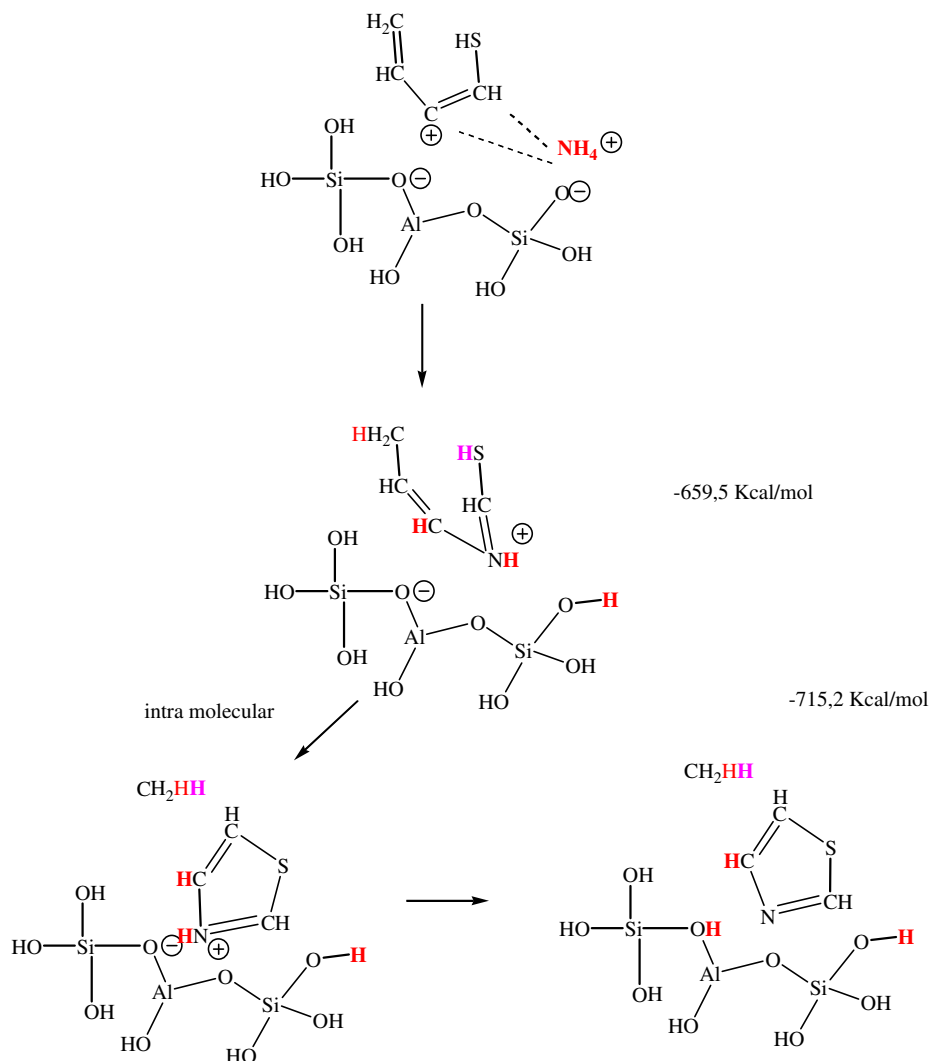


Fig. 24. Final conformation of the ammonium intermediary with the NH^+ moiety (Form 3). Protonated thiazole and methyl coordinated to the surface (Form 4), with final desorption of methane and thiazole.

The reaction standard enthalpies for the generation of the forms from the thiophene molecule far away from the active site model are calculated using the known formula:

$$\Delta H_{\text{reaction}}^0 = \sum \Delta H_{\text{products}}^0 - \sum \Delta H_{\text{reactives}}^0 \quad (11)$$

being $\Delta H_{\text{products}}^0$ the formation enthalpy of the selected form, and $\Delta H_{\text{reactives}}^0$ the formation enthalpies of the thiophene molecule and the active site shown in Fig. 22. These formation energies were found by the PM3 minimization calculations.

The MM2/PM3 calculation involve several steps that lead to the following forms: thiophene adsorbed near the Al–O–Si (Form 1), cationic thiophene species with positive charge on carbon 2 (Form 2a) or on carbon 3 (Form 2b), and alkoxide thiophene through carbon 2 (Form 2c) or carbon 3 (Form 2d).

For every form, from 1 to 2d, the enthalpy of formation is calculated and compared. Once the best situation is found, in the present case it is the form 2b (Fig. 23), the structure of an intermediate with the NH moiety added to thiophene is modeled, with the final conformation of the intermediary on the site called Form 3 (Fig. 24). This ammonium intermediary can direct to two new forms: (a) Form 4,

with the original simple site regenerated and release of methane and thiazole to the gas phase (Fig. 24) and (b) Form 5, with protonated thiazole and methyl coordinated to the surface (Fig. 25).

From Fig. 24 it is apparent that methane and thiazole should be observed as products in the gas phase if they desorbed, with generation of Form 4 at the surface. However, experimentally neither methane nor thiazole species are detected in the gas phase, with this finding suggesting that if methane and thiazole are formed, they keep adsorbed on the surface, thus ammonium intermediary evolves preferentially to Form 5 (Fig. 25).

Even if the results of the MM2 calculation plus the PM3 minimization step can be considered of semi-quantitative value, the following are relevant findings:

1. Cationic species with the positive charge on Carbon 3 (Form 2b) and the O from Al–O–Si negative are a preferred form with a reaction enthalpy close to 0. The alkoxide formation in C₂ or C₃ (Forms 2c and 2d) are endothermic by 14.2 and 33.3 Kcal mol⁻¹, respectively, being their formation severely hindered.
2. Generation of Form 3 (the ammonium form) is the most endothermic step of all, by 26.7 Kcal mol⁻¹.

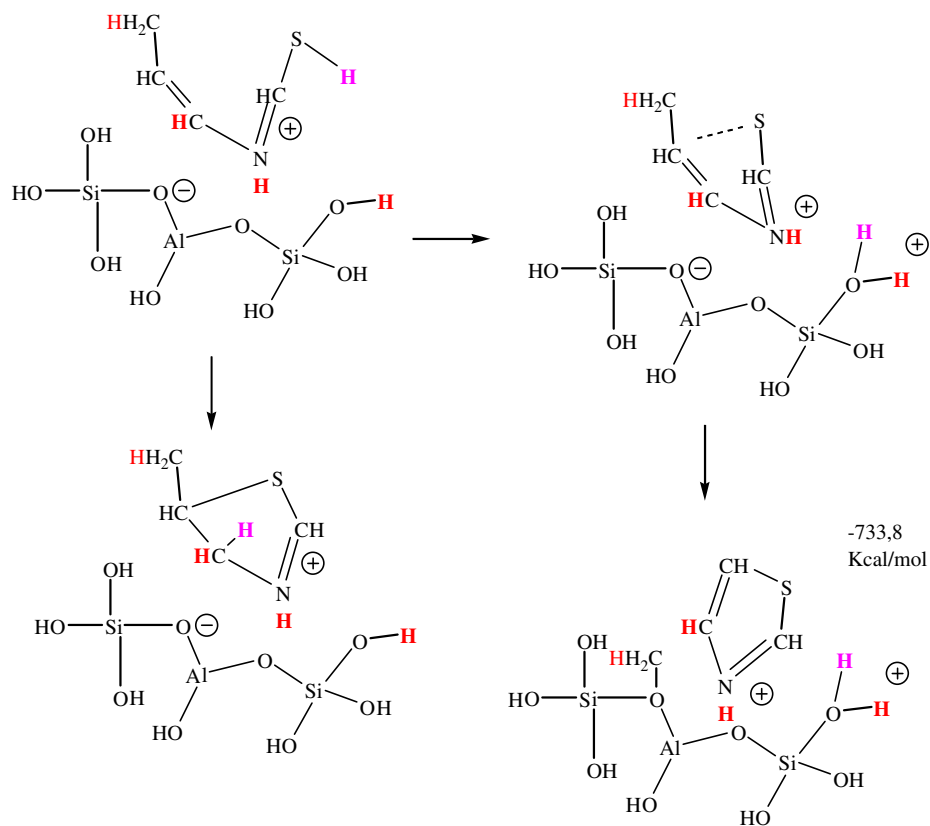


Fig. 25. Form 5 with thiazole protonated and methyl strongly adsorbed on surface.

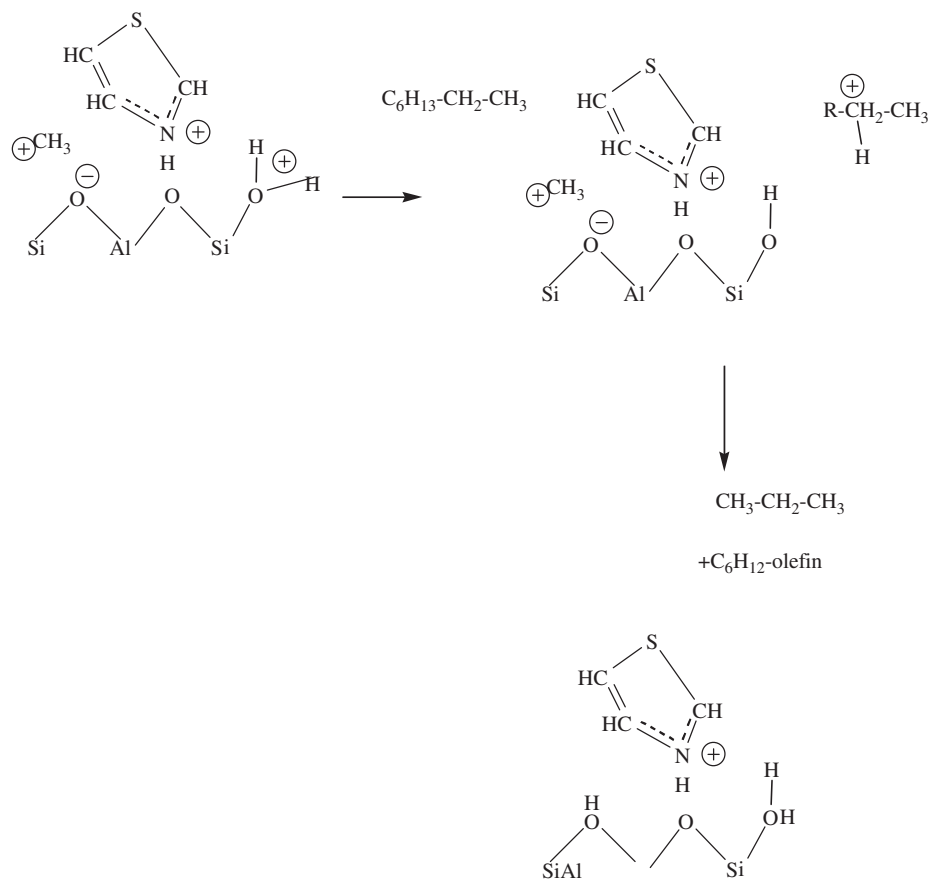


Fig. 26. Regeneration of active sites due to the hydrocarbon contribution.

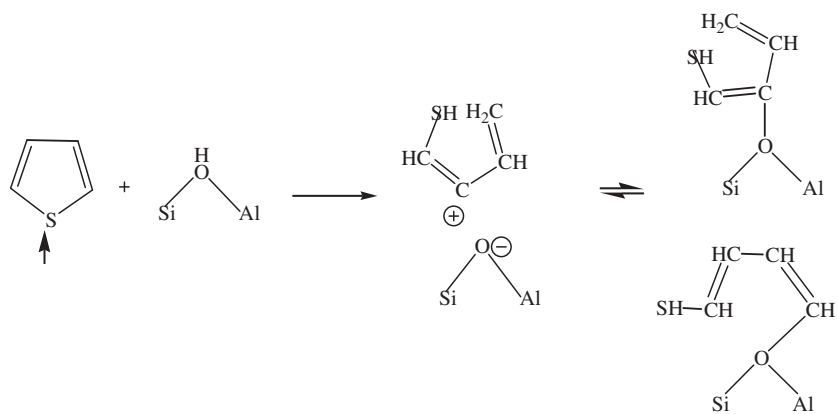


Fig. 27. Adsorption of thiophene in ionic species leading to ring opening.

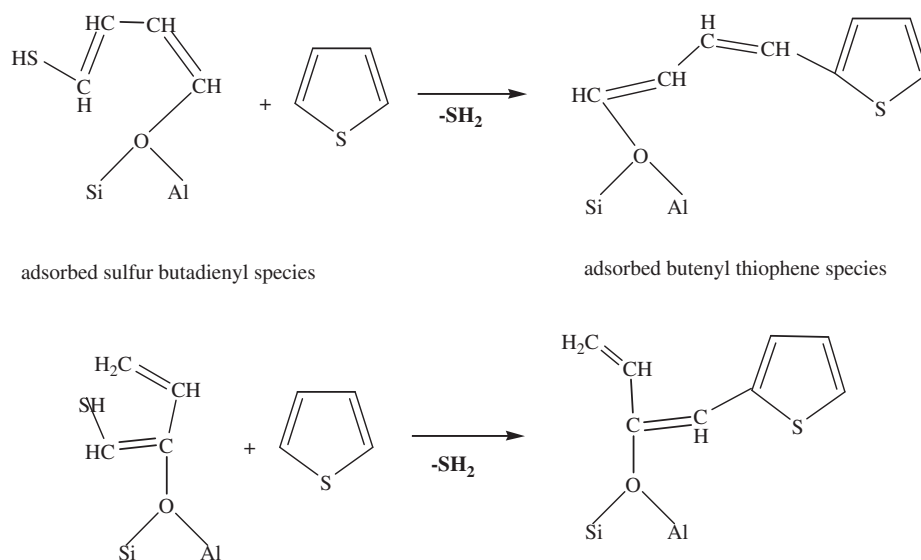


Fig. 28. Reaction of the adsorbed hydrogen sulfur butadienyl group with formation of hydrogen sulfide.

3. Generation of Form 5, with a reaction enthalpy of $-47.5 \text{ Kcal mol}^{-1}$ (very exothermic), is preferred pathway over formation of Form 4, due to the fact that the last one requires desorption of thiazole and methane, being this desorption endothermic by $18.7 \text{ Kcal mol}^{-1}$. This theoretical result agrees with the experimental findings of this study, where methane and thiazole are not observed in the gas phase product. Even more, the high amounts of methyl-thiophene found in the present experimental results, may be related to the proposed methyl group bonded to surface as a reactive species to react with a thiophene from gas phase.
4. Form 5, with protonated thiazole on the surface, a H_2O group bonded to one Si, and a methyl group adsorbed, could further react and generate other surface species, like those found in the coke analysis (Section 4.2.4).

On the other hands, the NH_4^+ groups adjacent to the acidic OH sites from the Si-OH-Al of ZSM5, can be considered as an additional source of H to the reacting hydrocarbon, with this additional H source able to regenerate the acidic Brønsted site, by reaction with the methyl group (Fig. 26).

4.4. Detailed mechanistic interpretation of thiophene conversion over H-ZSM5

Based on previous contributions, the thermodynamic analysis, and the experimental results, a mechanistic interpretation of thiophene removal over H-ZSM5 is proposed as described in Fig. 27. This mechanism involves the following: (a) interactions between thiophene and surface acidic OH groups, (b) thiophene ring opening with development of ionic species on the catalyst surface, and (c) formation of adsorbed sulfur butadienyl groups on the catalyst surface.

The experimental data obtained in the present study support the view that adsorbed thiophene species are associated with specific irreversible interactions between thiophene and surface acidic OH groups, as the ones described in Fig. 27. In this sense, the nitrogen observed in the sulfur adsorbed species (coke extract), as well as, the production of H_2S , can be interpreted via thiophene ring opening, with formation of ionic species on the surface as transition states leading to adsorbed sulfur butadienyl groups.

It is important to point out that, contrary to early interpretations (Jaimes et al., 2008), the conversion of the adsorbed sulfur

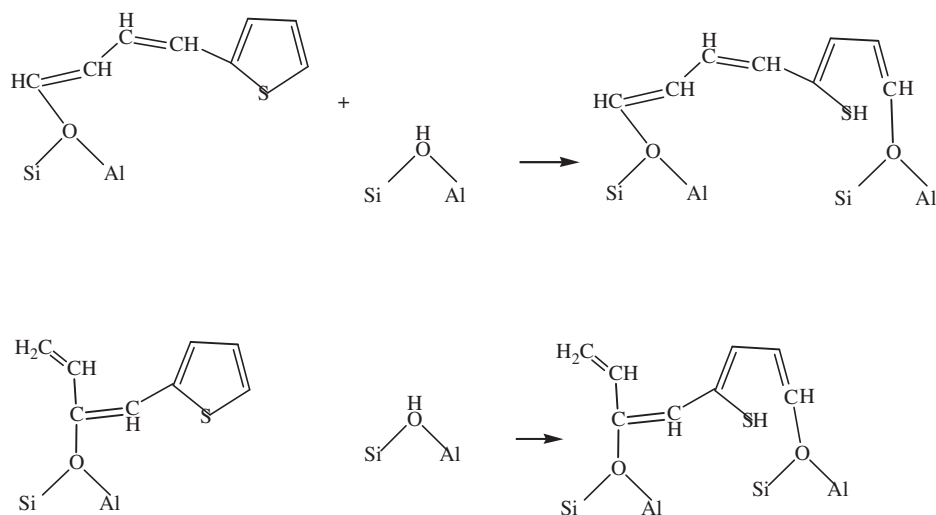


Fig. 29. Formation of adsorbed neighbor thiophene derived species.

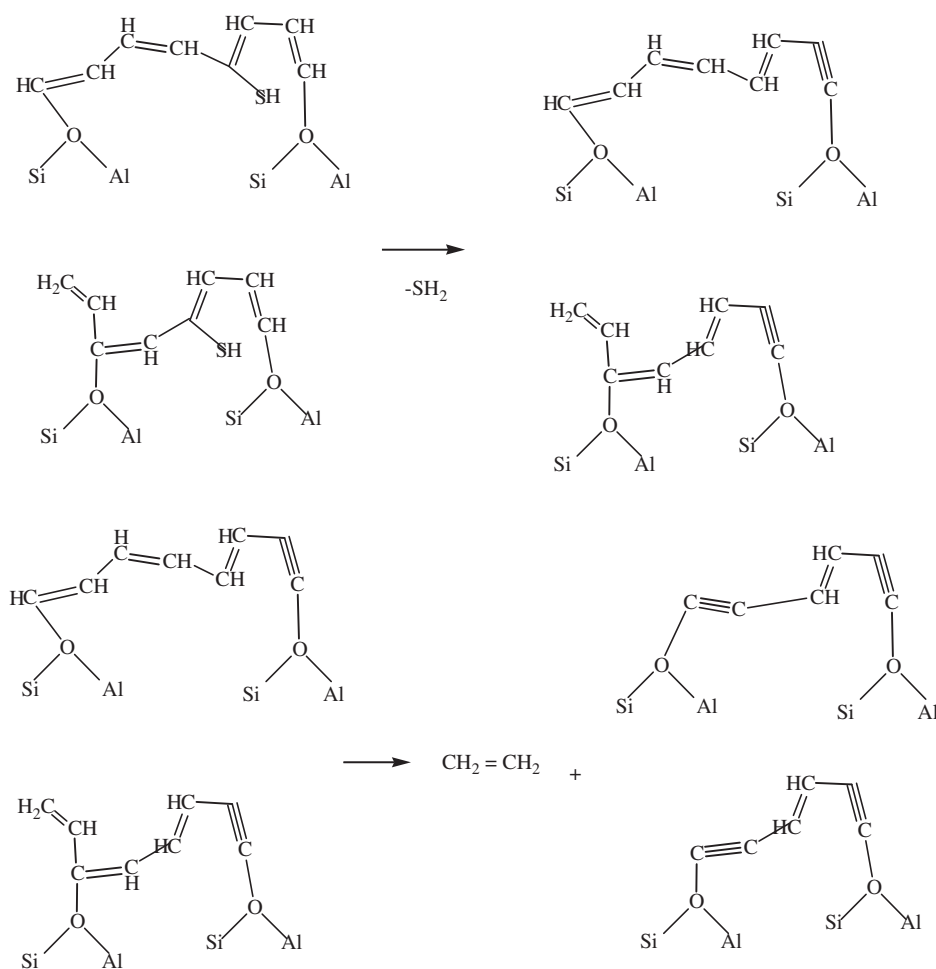


Fig. 30. Formation of ethylene via reaction of two adsorbed neighbor thiophene derived species.

butadienyl group into butadiyne was not observed in the experimental results, and thiophene dimers were not found in the coke analysis. This supports the view that alkoxide species intermediates are unlikely to be formed under the conditions studied.

Even more, the key adsorbed hydrogen sulfur butadienyl intermediate can undergo further reactions such as:

(a) Hydrogen sulfide formation from reaction of the adsorbed hydrogen sulfur butadienyl species and other thiophene molecule

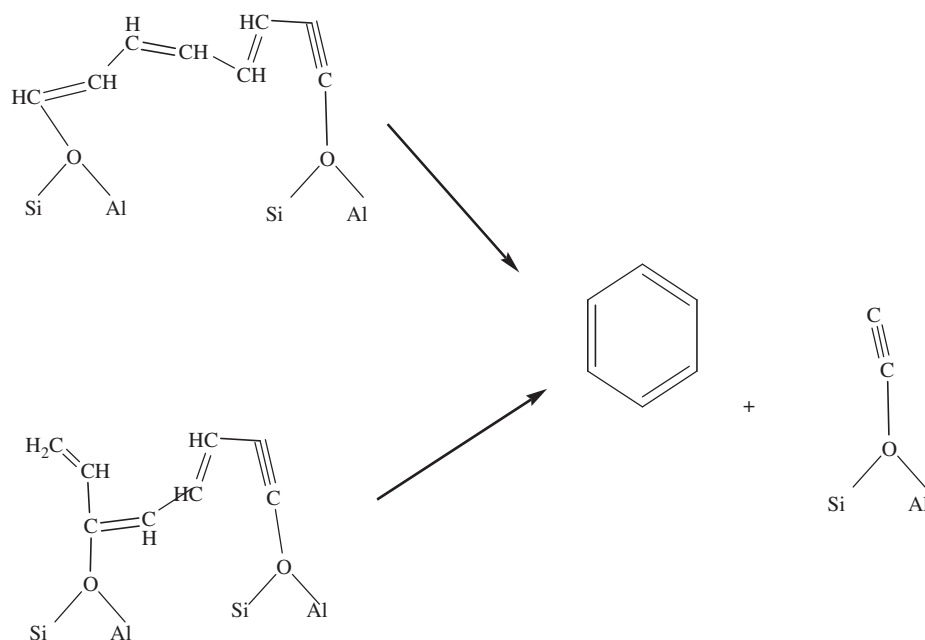


Fig. 31. Formation of benzene from two adsorbed neighbor thiophene derived species.

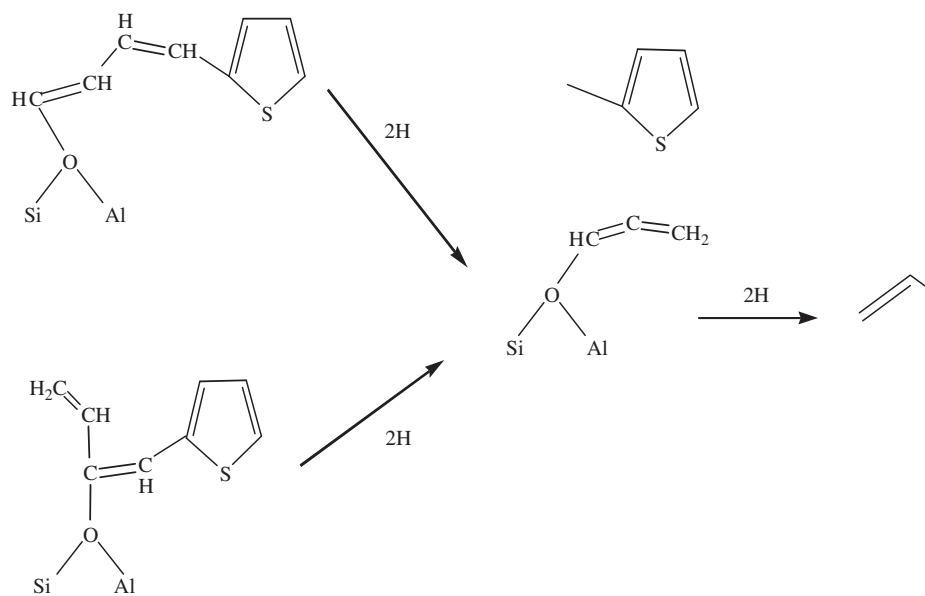


Fig. 32. Formation of methyl-thiophene from adsorbed butenyl thiophene species.

(Fig. 28). In this respect one should notice that desulfurized thiophene fragments on H-ZSM5 are highly unsaturated and unable to desorb as stable molecules without a separate source of hydrogen.

- Formation of ethylene via reaction of two adsorbed neighbor thiophene derived species (Figs. 29 and 30). Benzene can be formed via hydrogenation of thiophene fragments remaining after ring opening and H_2S evolution (Fig. 31).
- Propylene and methyl-thiophene formation via hydrogenation and cracking of adsorbed butenyl thiophene intermediary species (Fig. 32).
- Formation of benzothiophene via reaction of the adsorbed hydrogen sulfur butadienyl group with another thiophene molecule

by a Diels Alder reaction (Fig. 33). Benzothiophene is produced in an isolated Brönsted site.

As a result of the mechanism described above, the adsorbed butenyl thiophene intermediary, formed by reaction of thiophene with adsorbed sulfur butadienyl group on the surface, can suffer cracking and cyclization or reordering and hydrogenation. In this respect, when hydrogen is available in neighboring sites of the sulfur adsorbed species, the formation of propylene, methyl-thiophene, benzene, and ethylene is allowed. Evidence of this is shown in Section 4.2.1, where there is an increment in the production of H_2S , alkyl-thiophene species and aromatics at higher thiophene concentrations in the thiophene/*n*-octane reactant mixture. Alternatively,

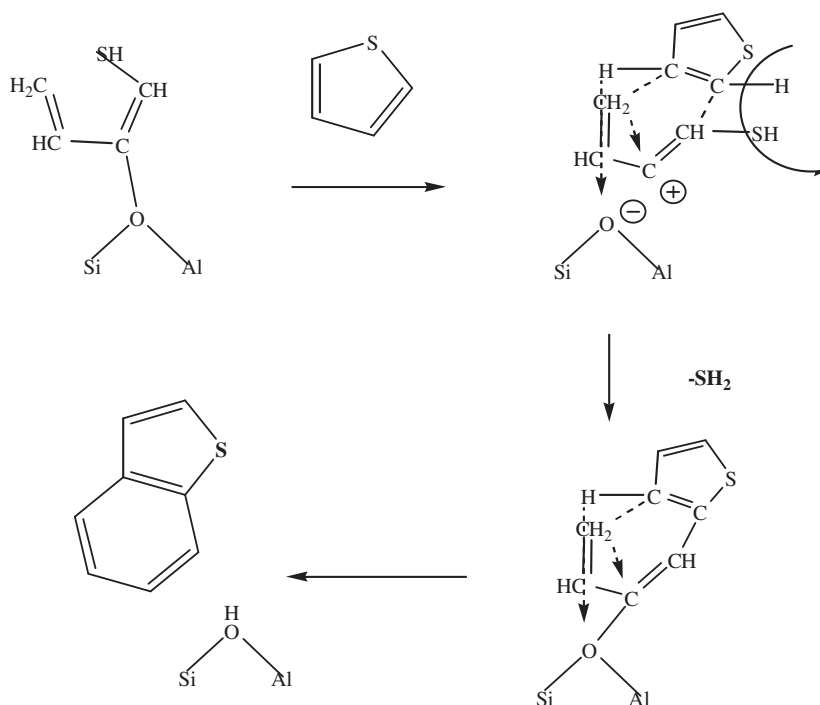


Fig. 33. Benzothiophene formation from a thiophene and an adsorbed thiophene derived species.

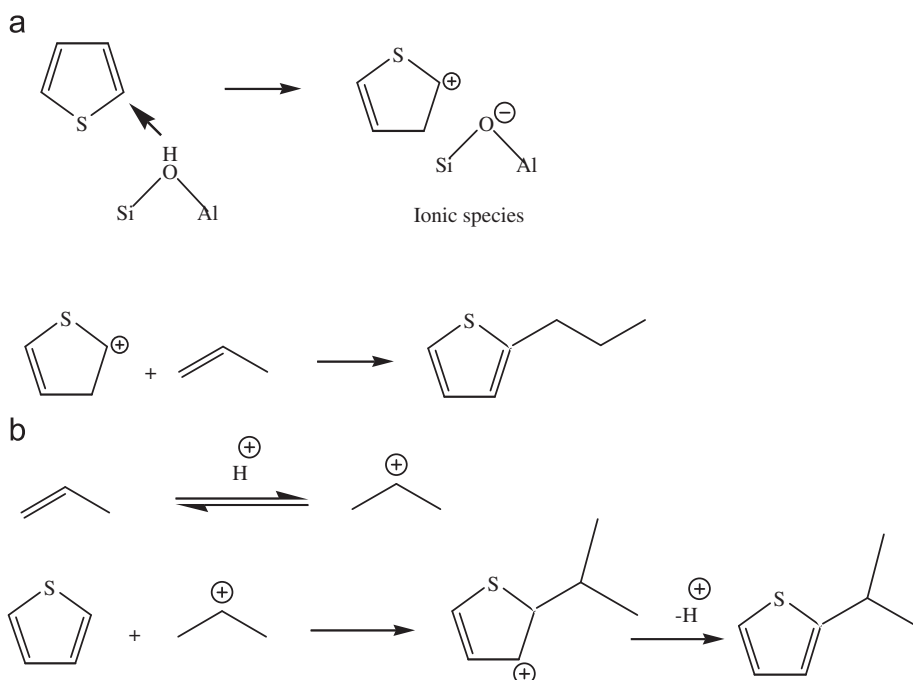


Fig. 34. Thiophene alkylation over H-ZSM5 via carbenium ion mechanisms.

if there is a severe deficiency of hydrogen, the tendency would be then to form benzothiophene and H_2S only, as it is found in pure thiophene over H-ZSM5 conversion experiments (refers to Section 4.2.3).

On the other hand and as observed in the experiments, not only thiophene ring opening but also thiophene alkylation reactions occurs (refer to Section 4.2.1). In this respect, *n*-octane can be considered as a hydrogen donor in the thiophene ring opening reactions

as well as a co-reactant in thiophene alkylation reactions, with its conversion on H-ZSM5 mainly leading to light olefins formation.

Alkylation of thiophene over H-ZSM5 can proceed via carbenium ion type mechanisms (Fig. 34). Even more, taking into consideration that both, linear and ramified alkyl-thiophenes were observed (refer to Table 1, and Appendix A), two alkylation pathways are suggested: (a) thiophene protonation on a Brønsted acid site, and reaction of the carbenium ion formed with an olefin to produce a linear

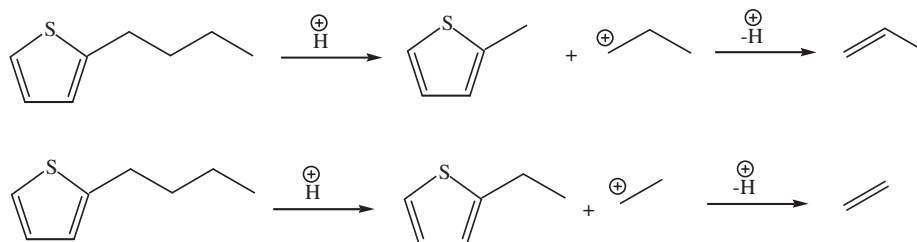


Fig. 35. Monomolecular reaction mechanisms of alkyl-thiophene cracking.

alkyl-thiophene (Fig. 34a) and (b) protonation of the olefin and reaction with a free thiophene molecule, leading to ramified alkyl-thiophenes (Fig. 34b). Similar mechanisms were reported for thiophene alkylation over faujasites zeolites (Valla et al., 2006; Richardeau et al., 2004).

Long chain alkylated thiophenes can be either the final product or can further react via monomolecular mechanisms. These mechanisms involve as described in Fig. 35, proton attack on a sigma C–C bond in the alkyl chain (protolytic cracking), to give an olefin and a short alkyl-thiophene. Furthermore, cyclization reaction of long chain alkyl-thiophenes to produce bicyclic compounds followed by dehydrogenation may also occur (reaction 10, Fig. 2), leading to benzothiophene or alkyl-benzothiophenes. One should notice that cyclization of long chain alkylated thiophenes is thermodynamically favored over cracking, as discussed in Section 2.

On the basis of the mechanisms proposed and of the experimental results of the present study, one can assert that thiophene conversion over H-ZSM5 proceeds via thiophene adsorption with ring opening, either via thiophene protonation and alkylation with olefins. In this respect, the free of sulfur hydrocarbons present in the gasoline can be considered as hydrogen providers as well as co-reactants in desulfurization reactions over zeolites.

5. Conclusions

The following are the most relevant conclusions of this research:

- The reaction equilibrium thermodynamic of thiophene conversion over zeolites is established to determine the most thermodynamically favored reaction pathways. This analysis shows that both thiophene hydrogenation and dimerization are thermodynamically constrained while thiophene alkylation and ring opening are preferred steps, with alkylation being favoured over hydrogen transfer.
- Experimental results obtained in a CREC fluidized riser simulator are in agreement with the thermodynamic analysis with no tetra-hydro-thiophene, thiophene dimers or butadiene being formed from thiophene cracking over H-ZSM5. Thiophene conversion leads mainly to coke, H_2S , aromatics, alkyl-thiophenes and benzothiophene.
- The derived reaction mechanisms suggest that adsorption and cracking of sulfur compounds on H-ZSM5 zeolites are very important steps. In this respect, a key role is assigned to the hydrogen sulfur butadienyl group. It is postulated on this basis, that thiophene conversion occurs according to selective adsorption of thiophene with formation of carbenium ions as transition states followed by thiophene ring opening, bimolecular reactions between 2 molecules of thiophene, with or without hydrogen transfer, or alkylation reactions.
- It is also proven that gasoline components can play a key role as hydrogen donors favouring critical steps that promote thio-

phene ring opening as well as contributing as co-reactants for alkylation.

- Conversion of thiophene in low sulfur content mixtures over H-ZSM5 shows significant levels of coke. Thus, a twin fluid-bed system involving a fluidized bed reactor and fluidized bed regenerator is needed for implementing a gasoline desulfurization process where catalyst activity is kept at high levels at all times.

Notation

ABD	average bulk density
C_p^0	specific heat, $J mol^{-1} K^{-1}$
Cat/oil	catalyst to oil ratio, g/g
$Coke_{cTh}$	converted thiophene ending in coke, %
CREC	chemical reaction engineering center
EPMA	electron probe microanalysis
FCC	fluid catalytic cracking
FID	flame ionization detector
FPD	flame photometric detector
FTIR	Fourier transformed infra red
Gas_{cTh}	converted thiophene ending in gas phase, %
$Gasoline_{cTh}$	converted thiophene ending in gasoline, %
GC	gas chromatography
IR	Infrared
K	equilibrium constant
MM2	molecular mechanics 2
MSD	mass selective detector
nC_8	<i>n</i> -octane
PM3	parameterized model 3
PSD	particle size distribution
Rx	reaction
S_{Th}	thiophene adsorption/conversion selectivity
T	temperature, K
Th	thiophene
TIC	MSD signal
TPD	temperature programmed desorption
W_{H_2S}	mass fraction of H_2S in product stream
W_i	total mass fraction of sulfur species <i>i</i> that fall into the gasoline ebullition range
W_{Th}, W_{nC_8}	mass concentration of thiophene and <i>n</i> -octane in reactant mixture
XRD	X-ray diffraction
X_{Th}, X_{nC_8}	conversion of thiophene and <i>n</i> -octane, respectively, %
$\Delta G_{rxn,T}^0$	Gibbs free energy of reaction, $kJ mol^{-1}$
$\Delta G_{f,T}^0$	Gibbs free energy of formation, $kJ mol^{-1}$
ΔH_f^0	enthalpy of formation, $kJ mol^{-1}$
$\Delta H_{rxn,298}^0$	enthalpy of reaction, $kJ mol^{-1}$
\sum	sums the product of number of times a group appears in the compound and the group contribution value

Acknowledgments

M.L. Ferreira would like to acknowledge the financial support from CONICET (Argentina). H. de Lasa and L. Jaimes would also like to recognize the valuable funding provided by NSERC (Canada).

Appendix A.

Conversion and product distribution of catalytic runs with thiophene and *n*-octane mixtures at cat/oil of 5, reaction times of 5, 10,

Table A1

Conversion and products distribution from catalytic conversion of thiophene/*n*-octane mixtures at 450 °C, 5 wt% thiophene, and catalyst/feedstock = 5.

Reaction time (s)	5	10	15	20
<i>Hydrocarbon products distribution (wt%)</i>				
C ₂ 's	0.41	0.84	1.30	1.57
C ₃ 's	3.97	5.92	8.13	10.48
isoC ₄	0.75	1.26	1.98	2.58
<i>n</i> C ₄	1.55	2.47	3.83	4.36
C ₄ =	1.26	1.99	2.22	2.35
C ₅	0.28	0.50	1.13	2.35
C ₅ =	0.44	0.78	0.99	1.16
<i>n</i> C ₈	85.67	80.42	74.10	68.59
Toluene	0.36	0.7363	1.1215	1.52
Alkylbenzene	0.27	0.54	1.18	1.40
<i>Sulfur products distribution (ppm)</i>				
H ₂ S	135	231	284	333
Thiophene (wt%)	4.98	4.43	3.83	3.38
Methyl thiophene	249	494	718	994
Ethyl thiophene	175	303	469	686
2-(1Methyl ethyl) thiophene	35	162	239	315
2-Propyl thiophene	47	67	120	177
2-Butyl thiophene	0	14	34	43
Benzothiophene	4	12	24	31
Coke (%) (wt coke/wt cat)	0.01	0.03	0.05	0.07
H ₂ S/(alkyl-Th+benzo-Th) ^a	0.83	0.70	0.57	0.47
<i>n</i> C ₈ conversion (%)	9.61	15.24	21.98	27.85
Thiophene conversion (%)	5.54	16.15	27.46	36.03
Thiophene conversion selectivity (S _{Th})	10	19	22	23

^aMole ratio.

Table A2

Conversion and products distribution from catalytic conversion of thiophene/*n*-octane mixtures at 400 °C, 5 wt% thiophene, and catalyst/feedstock = 5.

Reaction time (s)	5	10	15	20
<i>Hydrocarbon products distribution (wt%)</i>				
C ₂ 's	0.00	0.00	0.37	0.57
C ₃ 's	2.30	3.98	6.08	7.40
isoC ₄	0.58	1.06	1.67	2.20
<i>n</i> C ₄	1.05	2.00	3.10	3.86
C ₄ =	0.56	1.42	2.34	2.70
C ₅	0.00	0.46	0.74	1.29
C ₅ =	0.14	0.59	0.77	0.98
<i>n</i> C ₈	90.26	85.85	79.93	76.02
Toluene	0.00	0.00	0.29	0.48
Alkylbenzene	0.00	0.00	0.36	0.50
<i>Sulfur products distribution (ppm)</i>				
H ₂ S	30	59	103	128
Thiophene (wt%)	5.08	4.58	4.24	3.82
Methyl thiophene	82	297	471	862
Ethyl thiophene	43	155	236	411
2-(1Methyl ethyl) thiophene	27	92	116	194
2-Propyl thiophene	28	37	90	117
2-Butyl thiophene	0	5	13	21
Benzothiophene	1	6	11	19
Coke (%) (wt coke/wt cat)	0.01	0.02	0.04	0.05
H ₂ S/(alkyl-Th+benzo-Th) ^a	0.54	0.31	0.35	0.25
<i>n</i> C ₈ conversion (%)	4.75	9.48	15.78	19.96
Thiophene conversion (%)	3.56	13.17	19.74	27.70
Thiophene conversion selectivity (S _{Th})	13	25	22	25

^aMole ratio.

15, and 20 s, and temperatures of 400 and 450 °C are reported in Table A1 and A2.

Both Tables A1 and A2 show the characteristic consistent mechanistic patterns at two temperatures and four residence times (5, 10, 15, and 20 s) described in Section 4.2.1.

Additionally, and as expected, *n*-octane and thiophene conversion increase progressively with reaction time in the 5–20 s range and temperature, reaching a maximum value of 28% and 36%, respectively, at 450 °C and 20 s.

References

- Atias, J.A., Tonetto, G., de Lasa, H., 2003. Modeling fluid catalytic cracking in a novel CREC riser simulator: adsorption parameters under reaction conditions. *International Journal of Chemistry Reactor Engineering A* 50, 1–24.
- Babich, I.V., Moulijn, J.A., 2003. Science and technology of novel processes for deep desulfurization of oil refinery streams: a review. *Fuel* 82, 607–631.
- Bartholomew, C.H., Fuentes, C.A., Guisnet, M., Magnoux, P., Martin, D., 1997. Roles of acidity and pore structure in the deactivation of zeolites by carbonaceous deposits. *Catalyst Deactivation*, 1–20.
- Belliere, V., Geantet, Ch., Vrinat, M., Ben-Taarit, Y., Yoshimura, Y., 2004. Alkylation of 3-methylthiophene with 2-methyl-2-butene over a zeolitic catalyst. *Energy and Fuels* 18, 1806–1813.
- Chica, A., Strohmaier, K.G., Iglesia, E., 2004. Adsorption, desorption, and conversion of thiophene on H-ZSM5. *Langmuir* 20, 10982–10991.
- Chica, A., Strohmaier, K.G., Iglesias, E., 2005. Effects of zeolite structure and aluminum content on thiophene adsorption, desorption, and surface reactions. *Applied Catalysis B: Environmental* 60, 223–232.
- de Lasa, H., 1992. Riser Simulator. US Patent 5 102 628.
- de Lasa, H., Hernandez, R., Tonetto, G., 2006. Catalytic desulfurization of gasoline via dehydrosulfidation. *Industrial & Engineering Chemistry Research* 45, 1291–1299.
- Delitala, C., Cadoni, E., Delpiano, D., Meloni, D., Melis, S., Ferino, I., 2008. Liquid-phase thiophene adsorption on MCM-22 zeolite and activated carbon. *Microporous and Mesoporous Materials* 110, 197–215.
- Deng, Y., White, G.N., Dixon, J.B., 2002. Effect of structural stress on the intercalation rate of kaolinite. *Journal of Colloid and Interface Science* 250, 379–393.
- Elanaya, M., Koyama, M., Kubo, M., Broclawik, E., Miyamoto, A., 2005. Periodic density functional investigation of Lewis acid sites in zeolites: relative strength order as revealed from NH₃ adsorption. *Applied Surface Science* 246, 96–101.
- Franklin, J.L., 1949. Prediction of heat and free energies of organic compounds. *Industrial and Engineering Chemistry* 41, 1070–1076.
- Fu, J., Wang, P., He, M.Y., 2000. Reaction chemistry related to FCC gasoline sulfur reduction. *American Chemical Society Preprint Division Petrochemical* 45, 697–700.
- Garcia, C.L., Lercher, J.A., 1992. Adsorption and surface reactions of thiophene on ZSM5 zeolites. *Journal of Physical Chemistry* 96, 2669–2675.
- Garcia, C.L., Lercher, J.A., 1993. Hydrogen bonding of sulfur containing compounds adsorbed on zeolite HZSM5. *Journal of Molecular Structure* 293, 235–238.
- Geldart, D., 1973. Types of gas fluidization. *Powder Technology* 7, 285–292.
- Guisnet, M., Magnoux, P., 1989. Coking and deactivation of zeolites influence of the pore structure. *Applied Catalysis* 54, 1–27.
- Jaimes, L., Tonetto, G., Lujan, M., de Lasa, H., 2008. Desulfurization of FCC gasoline: novel catalytic processes with zeolites. *International Journal of Chemical Reactor Engineering* 6, 1–66.
- Joback, K.G., Reid, R.C., 1987. Estimation of pure-component properties from group-contributions. *Chemical Engineering Communications* 57, 233–243.
- Li, W., Yu, S.Y., Iglesia, E., 2001. Isotopic tracer studies of thiophene desulfurization reactions using hydrogen from alkanes on H-ZSM5 and Co/H-ZSM5. *Journal of Catalysis* 203, 175–183.
- Poling, B.E., Prausnitz, J.M., O'Connell, J.P., 2001. *The Properties of Gases and Liquids*, fifth ed. McGraw-Hill, USA.
- Richardeau, D., Joly, G., Canaff, C., Magnoux, P., Guisnet, M., Thomas, M., Nicolaos, A., 2004. Adsorption and reaction over HFAU zeolites of thiophene in liquid hydrocarbon solutions. *Applied Catalysis A: General* 263, 49–61.
- Saintigny, X., van Santen, R.A., Clémendot, S., Hutschka, F., 1999. A theoretical study of the solid acid catalyzed desulfurization of Thiophene. *Journal of Catalysis* 183, 107–118.
- Shan, H.H., Li, C.Y., Yang, C.H., Zhao, H., Zhao, B.Y., Zhang, J.F., 2002. Mechanistic studies on thiophene species cracking over USY zeolite. *Catalysis Today* 77, 117–126.
- Smirniotis, P.G., Ruckenstein, E., 1994. Comparison of the performance of ZSM-5, β zeolite, Y, USY, and their composites in the catalytic cracking of *n*-octane, 2,2,4-trimethylpentane, and 1-octene. *Industrial Chemical Engineering Research* 33, 800–813.
- Stull, D., Westrum, E., Sinke, G., 1969. *The Chemical Thermodynamics of Organic Compounds*. John Wiley & Sons, USA.
- Valla, J.A., Lappas, A.A., Vasalos, I.A., 2006. Catalytic cracking of thiophene and benzothiophene: mechanism and kinetics. *Applied Catalysis A: General* 297, 90–101.
- van Krevelen, D.W., Chermier, H.A.G., 1951. Estimation of the free enthalpy (Gibbs free energy) of formation of organic compounds from group-contributions. *Chemical Engineering Science* 1, 66–80.

- Wang, P., Fu, J., He, M.Y., 2000. Cracking-desulfurization of thiophene contained paraffin over zeolites. *Petroleum Processing and Petrochemicals* 31, 58–62.
- Welters, W.J., de Beer, V.H., van Santen, R., 1994. Influence of zeolite acidity on thiophene hydrodesulfurization activity. *Applied Catalysis A: General* 119, 253–269.
- Xu, Y., Shu, Y., Liu, Sh., Huang, J., Guo, X., 1995. Interaction between ammonium heptamolybdate and NH₄ZSM-5 zeolite: the location of Mo species and the acidity of Mo/HZSM-5. *Catalysis Letters* 35, 233–243.
- Yin, C., Xia, D., 2004. A study of the distribution of sulfur compounds in gasoline produced in China: Part 3. Identification of individual sulfides and thiophenes. *Fuel* 83, 433–441.
- Yu, S.Y., Li, W., Iglesia, E., 1999. Desulfurization of thiophene via hydrogen transfer from alkanes on cation-modified H-ZSM5. *Journal of Catalysis* 187, 257–261.